THESIS FOR THE DEGREE OF DOCTOR OF PHILOSOPHY

Calcium Battery Electrolytes: Strengths, Adversities and Leveraging Trajectories

JOHANNA TIMHAGEN

Department of Physics

CHALMERS UNIVERSITY OF TECHNOLOGY

Göteborg, Sweden 2026

Calcium Battery Electrolytes: Strengths, Adversities and Leveraging Trajectories

JOHANNA TIMHAGEN
ISBN 978-91-8103-389-2

Acknowledgements, dedications, and similar personal statements in this thesis, reflect the author's own views.

Doktorsavhandlingar vid Chalmers tekniska högskola
Ny serie nr 5846
ISSN 0346-718X
https://doi.org/10.63959/chalmers.dt/5846

Department of Physics
Chalmers University of Technology
SE-412 96 Göteborg
Sweden
Telephone + 46 (0)31-772 1000

Cover:
SEM image of calcium deposition on a stainless steel electrode by a KOTf-based electrolyte.

Chalmers Digital Printing
Göteborg, Sweden 2026

Calcium Battery Electrolytes: Strengths, Adversities and Leveraging Trajectories

JOHANNA TIMHAGEN
Department of Physics
Chalmers University of Technology

Abstract

Calcium metal batteries (CMBs), a promising next generation battery technology, have gained research interest over the last decade. CMBs are attractive for the prospect of a more sustainable chemistry, given the large abundance of Ca in the Earth's crust, and the high energy density, linked to their anodes' low electrochemical potential and large volumetric capacity. Ca metal anodes, however, are prone to form unwanted passivation layers, a phenomenon heavily influenced by the CMB electrolyte chemistry, making clever electrolyte design choices vital.

This thesis foremost covers two CMB electrolyte concepts. The first is solvent-free electrolytes in the form of molten salt electrolytes (MSEs), *i.e.* binary and multi-component systems of inorganic cations and anions, for which we explore how degradation can possibly be avoided. The second is dual-salt electrolytes, where the complex interplay between boron and K^+-ions alters and hopefully enhances electrochemical performance. Furthermore, the large implications of varying purity for commercially sourced Ca-salts are explored, as this can be detrimental to early-stage assessments of battery technologies in their infancy, such as CMBs.

The thermal properties of salts and electrolytes were evaluated by thermal gravimetric analysis (TGA) and differential scanning calorimetry (DSC), while local structure, particularly the entropic stabilization of MSEs and the ion-ion and ion-solvent interactions in liquid electrolytes, was explored by Raman spectroscopy. Finally, electrochemical performance was evaluated primarily using symmetric Ca||Ca cells, and, taken altogether, we generated data and creative ideas for advancing and expanding knowledge of various CMB electrolyte designs.

Keywords: calcium batteries, multivalent batteries, liquid electrolytes, molten salt electrolytes, eutectic electrolytes

List of Publications

The following papers are included in this thesis:

I **Local Structure and Entropic Stabilization of Ca-Based Molten Salt Electrolytes**
J. Timhagen, C. C. Cardona, J. Weidow and P. Johansson
Batteries & Supercaps 2024, 7, e202400297, doi.org/10.1002/batt.202400297

II **Molten salt electrolyte based high-temperature calcium metal batteries?**
J. Timhagen, A. Ponrouch, J. Weidow and P. Johansson
Submitted

III **Facilitating calcium metal batteries by potassium-containing electrolytes**
J. Timhagen, N. T. Luong, T. Hosaka, Z. Slim, J. Weidow and P. Johansson
In manuscript

IV **Next generation battery salt sourcing – the example of calcium bis(fluorosulfonyl)imide ($Ca(FSI)_2$)**
J. Timhagen, J. Weidow and P. Johansson
Under review

V **Successes and failures predicting the solubility of solid electrolyte interphase (SEI) species**
J. Timhagen, V. Thangavel, J. Forero Saboya, J. Weidow and P. Johansson
Electrochimica Acta 2025, 539, 147051, 10.1016/j.electacta.2025.147051

Declaration of author contribution

I JT performed all the experimental work and wrote the first draft of the manuscript. CCC performed all computational work and wrote the corresponding part of the first draft. All authors participated in revisions of the final manuscript.

II JT performed all the experiments and wrote the first draft of the manuscript. All authors participated in revisions of the final manuscript.

III JT designed the study, performed all the experimental work and wrote the first draft. NTL performed all computational work and deconvoluted the Raman and FTIR spectra. TH synthesised the Ca(BF4)2 salt. ZS provided guidance and support for the initial experiments. All authors participated in revisions of the final manuscript.

IV JT performed all the experiments and wrote the first draft of the manuscript. All authors participated in revisions of the final manuscript.

V JT performed the DSC experiments. VT performed DFT and COSMO-RS calculations and wrote parts of the original draft. JFS performed the ICP-MS experiments. JT composed and analysed the combined data and finished the original draft. All authors participated in revisions of the final manuscript.

List of Acronyms

AGG	Aggregates
BDM	Bockris-Devanthan-Müllen model
CE	Counter Electrode
CEI	Cathode Electrolyte Interphase
CIP	Contact Ion Pair
CMB	Calcium Metal Battery
COSMO-RS	Conductor-like Screening Model for Real Solvents
CV	Cyclic Voltammetry
DFT	Density Functional Theory
DMAc	Dimethylacetamide
DMSO	Dimethyl Sulfoxide
DN	Donor Number
DSC	Differential Scanning Calorimetry
EDL	Electric Double Layer
ESW	Electrochemical Stability Window
EV	Electric Vehicle
FTFSI	(Fluorosulfonyl)-(trifluoromethane-sulfonyl)imide
FTIR	Fourier-Transform Infrared
FSI	Bis(fluorosulfonyl)imide
GC	Galvanostatic Cycling
HEA	High Entropy Alloy
HCE	Highly Concentrated Electrolyte
IHP	Inner-Helmholtz plane
LIB	Lithium-Ion Battery
MD	Molecular Dynamics
MSE	Molten Salt Electrolyte
NFSI	Bis(nonafluorobutanesulfonyl)imide
NGB	Next Generation Battery
OHP	Outer-Helmholtz plane
OTf	Triflate
PTCDI	Perylene-3,4,9,10-tetracarboxylic diimide
SEI	Solid Electrolyte Interphase
SHE	Standard Hydrogen Electrode
SSIP	Solvent-Separated Ion Pairs
RDS	Rate Determining Step
RE	Reference Electrode
TFSI	Bis(trifluoromethylsulfonyl)imide
TGA	Thermal Gravimetric Analysis
WE	Working Electrode

Acknowledgements

"The cure for anything is salt (water): sweat, tears or the sea." - Isak Dinesen

First, I would like to express my deepest thanks to my supervisor, Patrik Johansson, for taking a chance on me. With my background in mechanical and materials engineering, not many would have let me into a Department of Physics. Thank you also for pushing me and encouraging me when my motivation for molten salt electrolytes was dwindling. And for allowing me the freedom to pursue other types of electrolytes as well, which certainly were outside the grant scope. With your resounding positivity, you taught me to be a researcher who always looks on the bright side.

I would also like to thank my co-supervisor, Jonathan Weidow, who is not only the most impressive runner I know but also always has a knack for putting things in their proper perspective. Thank you also to my examiner, Aleksandar Matic, for always lifting spirits with a well-placed joke and, year after year, ensuring that this division remains one of the greatest. To Alexandre Ponrouch and his group at ICMAB in Barcelona – thank you for generously welcoming me to the group, especially during a time when I was struggling. The time I spent there genuinely changed my outlook on life.

Nothing would run as smoothly as it does without Ezio Zanghellini – thank you for always providing a helping hand and for so freely sharing all your expertise. Equally, on the organizational side, a great thank you to Patricia Huijbers for providing insightful comments on first drafts and answering all my questions about what it is like to be a scientific project leader – you are an inspiration both professionally and as a human being.

The MF division has, from start to finish, felt like the best place to be, and that is all thanks to all smart, kind, and curious colleagues, both past and current. Thank you for all the chats over lunch and fika, great discussions during Batt-meetings, and fun times at the MF retreats. A big thanks to the members of the Best Office: Martina and Josef – who were my supporting office mates from the start - and to Auðunn, who brightened the office later and is here at the finish line.

For all the struggles in the lab and in interpreting data, it has been invaluable to always have kind and supportive people to turn to, a big thanks to Clément, Tomo, and Tan – and, in particular, Zaher, for also helping me get started with Ca metal, providing guidance and pushing me to go deeper with challenging questions. The biggest gift has been getting to know, laugh, and travel the world with Carolina and Mirna – thank you for the emotional support, the gossip sessions, and always being just a phone call away.

To my very dearest friends I made on my very first day at Chalmers over a decade ago, you initially met a very different version of me and have stood by me through all the ups and downs. I am so thankful to have you in my life and to be there to witness each other's greatest hits and biggest failures. A special mention and heartfelt thank you to Cornelia, who more than anyone has shown me the strength of friendship. Thank you also to the

Mölnlycke gang, for always making me shed tears of laughter. Becoming such great friends in the relatively short time we worked together is not guaranteed, and having the chance to keep them is really special.

A big thank you to both sides of my extended family for the lively birthday parties and the great meals shared. Thank you mormor, for keeping our large family together and checking in by text, something truly impressive for someone in their 90s. Thank you farmor, for staying curious and being genuinely interested in my research.

And finally, a great thank you to my family – mamma, pappa, and Albin – for all your support throughout these years. Too much can be said, but perhaps the greatest thanks of all goes to the love of the written word that you instilled in me - I do not think I would have gotten to this point without it.

TABLE OF CONTENTS

Chapter 1

Introduction

Worth your salt: To be competent and deserving of respect or pay for your work

The last time you cooked dinner, you more than likely added salt to your dish. Forgetting to do so typically results in a bland and dreary meal. As central as the salt is to the food on your plate, as central is the salt(s) to the electrolyte in our batteries. This holds true for mature technologies, such as the lithium-ion battery (LIB), but is equally important – if not more so – for technologies in their infancy, such as the calcium metal battery (CMB). Combining the wrong salt with the wrong solvent initially deemed CMBs unfeasible.[1] A "blunder" which took 25 years to correct.[2] The advancement of CMBs comes at a momentous time; never have batteries been more in demand than they are now. As global energy consumption increases,[3] the desire does not only lie in more *of* them, but also to get more *out of* them. Requirements such as lower cost, higher energy and power density, higher safety, and longer life length are just the start of a long wish list. In using calcium (Ca) metal, the 5th most common element in the Earth's crust,[4] CMBs represent a next generation battery (NGB) technology that seeks to revive hope in batteries based on abundant raw materials.

Expanding the battery market with different NGB technologies creates the opportunity to tailor your battery to targeted applications – thus, getting the most out of both. The strength of Ca is its ability to enable multi-electron redox processes, in which two electrons are transferred per cation, which, combined with the exchange of intercalation anodes for metal anodes, promises far higher energy densities.[5] While Ca metal has a specific capacity lower than Li metal,[6] its volumetric capacity makes it particularly attractive – beneficial for applications such as electric vehicles (EVs), which typically have very limited internal space. The batteries in EVs also generate significant internal heat during operation, thus requiring cooling systems to maintain control and safety.[7,8] Batteries that operate at elevated temperatures (80-120 °C)[8] could possibly simplify their design, and Ca, which melts at 842 °C, is appealing as a first-level approximation. As Ca has a low electrochemical potential of -2.87 V *vs.* the standard hydrogen electrode (SHE), within *ca.* 0.1-0.2 V of that of Li, this could also be done at high operating voltages.[9]

To achieve the aspiration of making CMBs a serious contender – which working principles and considerations are presented in **Chapter 2** – the Ca metal anode must be paired with the appropriate cell components: the cathode, which is out of scope for this thesis, and the electrolyte, which is at the very heart of it. Both rely on each other for their individual development, and both are severely hindered by the Ca metal anodes' susceptibility to form insulating passivation layers.[10] The electrolyte, which enables charge

transfer inside the cell, needs to be conductive to ions and isolating to electrons. Enhancing its ability to do so, among other properties, is expanded upon in **Chapter 3**. In modern rechargeable batteries the cells are pushed to their utmost voltage limits, in which decomposition products stemming from the electrolyte form a new phase – the solid electrolyte interphase (SEI) – which, like the electrolyte, needs to be both conductive to ions and isolating to electrons to be beneficial. For Ca metal anodes, this layer is often also isolating to ions, completely stopping charge transfer. The layer must therefore be such that it works *with*, not *against* the charge transfer, making clever electrolyte design to be of utmost importance for practical CMBs.

There are two main electrolyte concepts explored in this thesis: the traditional route of liquid electrolytes, but with a twist, and the significantly less traditional, molten salt electrolytes (MSEs), aimed at room temperature and elevated temperature (80-120 °C) operation, respectively. A major challenge for Ca-containing electrolytes is the sluggish diffusion of Ca^{2+}, owing to strong coulombic interactions arising from its high polarizing power.[11] Tailoring the solvation structure of liquid electrolytes to facilitate Ca^{2+} mobility can be achieved by disrupting it, either with highly dissociating solvents,[12] by changing the anion type, or even by changing the cation type. In **Paper III**, all three ways are used. Electrolytes designed for high-temperature applications must meet strict safety requirements: they must have high thermal stability and low vapor pressure.[8] On a proof-of-concept level, the MSEs, of which thermal and structural properties are studied in **Paper I**, with the continuation of their electrochemical properties in **Paper II**, fulfill both demands.

Finding suitable Ca salts is tricky; insufficiently few are commercial, many have low solubility,[13] and plenty have issues with hydration. Therefore, it is of great importance that the salts bought commercially are up to standard. In **Paper IV**, the quality of commercially sourced salt is questioned, as five Ca salts of the same kind are compared and tested, to varying degrees of similarity. Studying the SEI layer at interfaces provides insight into which phases are beneficial and which are not. This has been done indirectly, in **Paper V**, through modelling using the conductor-like screening model for real solvents (COSMO-RS), which reveals its stability by looking at the solubility of simple organic salts in common electrolyte solvents. As this is an experiment-focused thesis, however, the molecular dynamics (MD) simulations and density functional theory (DFT) calculations, of **Papers I** and **III**, are excluded.

To realize the different electrolyte concepts, several techniques have been used, with the theoretical background presented in **Chapter 4** and the results from **Papers I-V**, together with unpublished work, are presented in **Chapter 5**. First, in **5.1**, thermal properties by thermal gravimetric analysis (TGA) and differential scanning calorimetry (DSC) are used to obtain single Ca salts decomposition temperatures (T_d) and melting temperatures (T_m), which are compared to those of alkali metal salts. Their differences and how they mix at varying levels of MSE complexity are highlighted. Then, using the vibrational spectroscopy techniques of Raman spectroscopy, the local structure of liquid electrolytes and MSEs is presented in **5.2**, focusing on their respective benefits and challenges, related to increasing salt concentration. These understandings then support the electrochemical observations in **5.3**, where galvanostatic cycling and cyclic voltammetry were used with the same electrolytes. Finally, in **5.4**, the impact salt quality has on liquid electrolytes and MSEs electrochemical performance is presented.

These results paint a picture of the strengths and adversities that developing Ca battery electrolytes face, as concluded in **Chapter 6**. While the aspirations of making batteries based on abundant raw materials are no longer completely out of reach; the right conditions, the right cathode, and, foremost, the right electrolyte still need to come together to make CMBs a serious contender. This thesis aims to do so, by leverage the trajectories of making CMBs *worth their salt – e.g.,* deserving of the time spent and the interest gained in the last decade – and will do so from the perspective of the electrolyte salt, which here is not for your taste buds but for enabling any electrochemical reaction to take place at all.

Chapter 2

Calcium Metal Batteries

Salt of the earth: Someone of good character, honest, and reliable

The reactivity of Ca metal makes it prevalent in its primitive role, *e.g.*, present in fossils, building materials, and vital processes within the human body – but not in its metallic form, which is also why patience is needed to develop CMBs. If the reactivity to passivation layers can be overcome, the promise lies in its abundance, improved safety, and multi-electron redox capability—qualities that, at their core, make Ca metal the *salt of the earth*. In this chapter, the principle of rechargeable batteries, the distinct properties of Ca metal anodes, and a brief outlook on the challenges of Ca cathode development are presented. While the structure and transport phenomena of electrolytes are left for **Chapter 3**, the interactions of electrolyte species at the place of action – interfaces – and the formation of their decomposition products at the interfaces – interphases – are introduced here. By the end of this chapter, the prerequisites of this silvery-yellow metal for battery application are hopefully better understood.

2.1 Principles of rechargeable batteries

A battery provides electric energy by converting chemical energy through spontaneous chemical reactions.[14] This is realized through three main components: the electrodes; one negative (anode) and one positive (cathode), and the electrolyte. Together, they form an electrochemical cell (**Figure 2.1**), in this case, a battery. The anode and cathode contain the battery's active materials and should always be kept physically apart to avoid short-circuiting. This is done by the separator, which is wetted with the electrolyte. The electrolyte's function is to shuttle ions between the electrodes, thereby enabling chemical reactions to occur at the electrolyte/electrode interfaces. Finally, the external circuit connects the two electrodes.[15]

Depending on charge or discharge process, rechargeable batteries will change which electrode is anode and which is cathode. To minimize confusion, the electrode that is negative during discharge is commonly referred to as the anode for rechargeable batteries, and vice versa for the cathode.[14] During *discharge*, the anode gives up electrons, which go through the external circuit to the cathode. At the same time, cations travel from the anode to the cathode through the electrolyte.

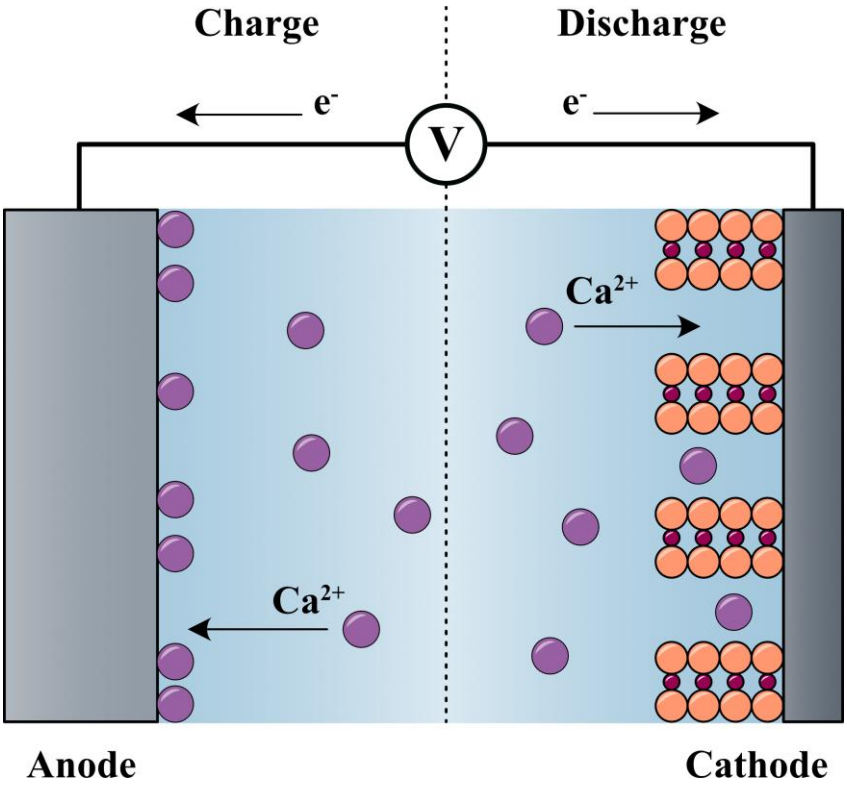

Figure 2.1 Electrochemical cell showing the electrolyte, the anode, and the cathode connected to an external circuit, during charge (left) and discharge (right).

Looking at *charging*, with the example of a cathode of $Ca_2FeSi_2O_7$,[16] the full reaction for a CMB can be written as,

$$Ca_2FeSi_2O_7 \rightarrow Ca(s) + CaFeSi_2O_7 \tag{2.1}$$

This reaction can be divided into two half-reactions: the reduction reaction at the anode – causing plating of calcium,

$$Ca^{2+} + 2e^- \rightarrow \mathrm{Ca(s)} \tag{2.2}$$

and the reduction reaction at the cathode,

$$Ca_2FeSi_2O_7 \rightarrow Ca^{2+} + 2e^- + CaFeSi_2O_7 \tag{2.3}$$

The amount of energy a battery can provide relies on how many ions the electrodes can accommodate and is referred to as the capacity,

$$Q = I \cdot t \tag{2.4}$$

where I is the current and t is the discharge time. The capacity is expressed in Ampere-hours (Ah) but is more practically expressed by the specific (gravimetric) capacity, which unit is capacity per electrode mass (often mAh/g). Furthermore, for any reaction to occur, it must be energetically favorable as described by the change in Gibbs free energy,

$$\Delta G = -nFE^\circ_{cell} \tag{2.5}$$

where F is the Faraday constant and n is the number of electrons taking part in the chemical reaction. $E°_{cell}$, is the cell voltage (V), *i.e.* the difference between the two electrodes standard reduction potentials,

$$E°_{cell} = (E_{red} - E_{ox}). \quad (2.6)$$

The energy (E) of the cell is then a function of the cell voltage and the capacity,

$$E = \int_0^Q E°_{cell}(q)dq. \quad (2.7)$$

The energy is expressed in Watt-hours (Wh) but is more often reported as the specific energy density (Wh/kg) or the volumetric energy density (Wh/L).

2.2 Anodes

There are basically three different types of anodes:[17] metal anodes, which are the focus of this thesis; intercalation anodes, which will be briefly discussed; and alloy- and conversion-reaction-based anodes, which are out of scope for this thesis. Intercalation anodes are made of host materials with open structures (**Figure 2.2a**) in which the ions intercalated associate via Coulombic bonding with the structure's conduction bands. As no redox reaction occurs, it has recently been suggested that intercalation anodes are not actually anodes, but rather "volumic capacitors".[18] Behind the realisation of LIBs is graphite, whose structure readily accommodates the small Li^+ ion,[19] but for NGB chemistries based on other cations, intercalation is trickier. Large ions such as K^+ have been successfully intercalated, though at the expense of distorting the structure and altering diffusion properties and interfacial compatibility.[20] Na^+, whose ionic radius lies between the two, struggles to desolvate from the electrolyte solvent due to its high Lewis acidity, making intercalation more troublesome.[17]

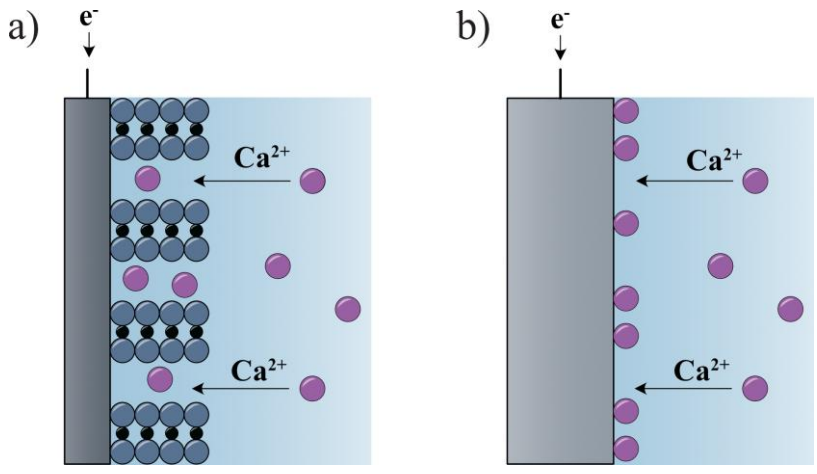

Figure 2.2 Energy storage through a) intercalation of ions and b) plating metal ions directly to the metal anode.

Multivalent cations, such as Ca^{2+}, Mg^{2+}, and Al^{3+}, hypothetically would require only half or one-third as many ions transferred to the host material to reach the same capacity as monovalent cations.[21] In reality, the mobility of multivalent ions is sluggish due to their charge, and, in the case of Ca^{2+}, is further affected by its relatively large ionic radius.[22]

Looking at a hypothetical Ca-ion battery with its readiness level extrapolated to that of LIBs shows performance lower than that of LIBs and would only be advantageous in terms of cost.[23]

Metal anodes, on the other hand, store energy by depositing the metal ions directly to the interface (**Figure 2.2b**), which occurs at a lower potential than intercalation. Exchanging graphite for metal anodes, such as Li or Ca metal, thereby promises far higher energy densities.[5] While Ca metal has a specific capacity (1 337 mAh/g) lower than Li metal (3 884 mAh/g), the stand-out appeal of Ca metal is its large volumetric capacity (2 073 mAh/cm^3),[6] which is comparable to that of Li (2 062 mAh/cm^3) – all values far beyond those of the prevailing graphite at 372 mAh/g and 841 mAh/cm^3. Metal deposition does not come without cost – the metal surface is inherently uneven, leading to irregularities. Upon charge, the roughest parts have the highest voltage and are where cations prefer to deposit, as it is more energetically favourable. This causes dendrites – needle-like structures that can grow to a length where the electrodes connect internally, leading to short-circuiting. During discharge, dendrites can break off, creating "dead" metal that is even more reactive and prone to dangerous outcomes.[19]

How susceptible a metal is to dendrite formation depends on its crystal structure, where body-centred cubic (Li, Na, K) are more prone, and face-centred cubic (Ca, Al) and hexagonal close-packed (Mg) are less so.[24] The applied current density, j, will also influence the deposited metal, which can be defined by the Butler–Volmer equation,

$$j = j_0 \left[e^{-\frac{\beta \eta F}{RT}} - e^{\frac{(1-\beta)\eta F}{RT}} \right] \tag{2.8}$$

where j_0 is the exchange current density, β is the charge-transfer coefficient, η is the applied overpotential, R is the universal gas constant, and T is the temperature.[25] For Ca, the morphology is typically interconnected plates, random fibres, or spherical aggregates.[26,27] The direction and extent of the reaction can be manipulated by changing the concentration of species in the electrolyte or the temperature of the cell. **Eq. 2.8** does, however, not consider diffusion in the electrolyte and thus assumes an abundance of species at the interface. This is only true during steady state, which occurs at a current density low enough so that the bulk electrolyte always has time to supply ions to the interface.[28] This is called the rate-determining step (RDS), controlled by mass-transfer, which differs from the charge transfer introduced in **Eq. 2.2**. While charge transfer is the process of electron relocation, *e.g.*, a change of property, mass-transfer is the physical transportation of ions or electrons into or out of the interfacial region. The current density at which the bulk electrolyte cannot supply enough ions to the interface is defined by the limiting current density,

$$j_{lim} = \frac{nFDC_0}{\delta} \tag{2.9}$$

where C_0 is the bulk concentration, D is the diffusion coefficient, and δ is the diffusion layer thickness.[28] When $j = j_{lim}$, the ions at the interfacial region are completely depleted. The time it takes to depletion, at a given constant current density, is given by the Sand's time,

$$\tau_{sand} = \pi D \left(\frac{nFC_0}{2j_0} \right)^2 \tag{2.10}$$

When the Sand's time is reached, the cell suffers instability, and dendrites start to grow.[28] Ca metal, which is less prone to dendritic growth due to its crystal structure,[24] is also less prone as the Ca^{2+} ions' mobility is sluggish and has strong Coulombic interactions with its surroundings,[27] thus, has a slower mass-transfer. This means that the time to depletion of ions at the interfacial region is slower, so that even at harsh conditions of $j > j_{lim}$, the initial plating is still dense and smooth, before any dendrites start to grow.[29] Li metal has shown dendritic growth at current densities as low as 1 mA/cm^2, while Ca metal sees no dendrite formation below 20 mA/cm^2,[30] which suggests that CMBs are safer for fast-charging.[27]

2.3 Cathodes

Cathode and electrolyte development for CMBs are each other's biggest bottlenecks – there is no standard electrolyte to validate new cathodes, just as there are no standard cathodes to validate new electrolytes. In contrast to the small Li^+ cation, which is readily hosted in inorganic structures, the high charge density and relatively larger size of the Ca^{2+} cation make it more challenging. Many of the cathodes tested for CMBs are therefore often organic, with more flexible structures and better electrochemical accessibility.[31] A good cathode for CMBs must not only have acceptably high intercalation voltage vs. Ca/Ca^{2+}, but it must also be thermodynamically stable – something troublesome to test with no standard electrolyte.[31] Many electrolytes dissolve the cathodes and passivate the Ca metal anode, hindering long-term cathode cycling. To get around this, symmetric cathode testing has been used: two full cells are first reduced, then disassembled, and finally cycled with only the cathodes, which allows a fair assessment of the cathodes.[32]

For Ca electrolyte testing in full cells, some have chosen perylene-3,4,9,10-tetracarboxylic diimide (PTCDI),[12,33] which is also the case in **Papers IV**. While PTCDI enables only a few cycles to verify electrolyte performance, the first cycle typically shows large irregularities due to initial cathode dissolution, which stabilizes in later cycles. Despite this, PTCDI remains a good enough comparable option for proof-of-concept in electrolyte testing for now.

2.4 Interfaces and interphases

An interface is the intersection between two physically distinct phases. It has its own unique set of properties, due to the electric charge build-up between the two phases, known as the electric double layer. As such, it does not behave as the bulk electrode or the bulk electrolyte.[34] When the electrolyte decomposes, the species attach to the electrode surfaces and begin to form an interphase, becoming a distinct phase. This means that the system now has one more interface – one between the electrode and the interphase, and one between the interphase and the electrolyte (**Figure 2.3**). The specific properties of interfaces are expanded upon in section **2.4.1** and those of the interphases in section **2.4.2**.

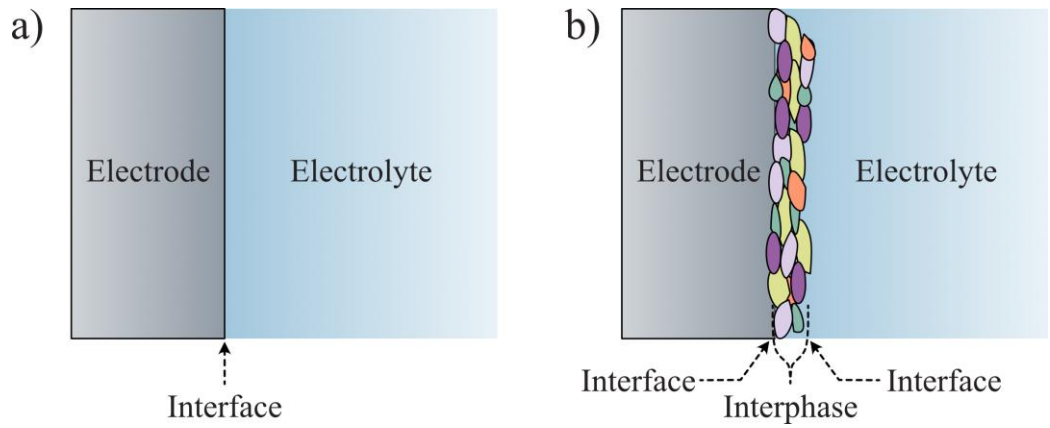

Figure 2.3 The intersection between electrode and electrolyte, where a) the interface, and b) the interphase.

2.4.1 The electronic structure of the interface

From the perspective of the electrons in the bulk electrode and the ions in the bulk electrolyte, the charge distribution is approximately symmetrical, meaning that the bulk of each phase remains electroneutral. Where the electrode and the electrolyte meet – the interface – the symmetry is broken in both, so that the ions directly at the electrode surface will feel a different electrical field than that of the ions in the bulk electrolyte. The same goes for the electrons in the electrode directly in contact with the electrolyte. Due to the breaking of symmetry, electroneutrality is broken too, which means a new regional equilibrium must arise. This region becomes an electrified surface, with the electrode bearing an excess of negative charges (electrons) and the electrolyte bearing an excess of positive charges (cations). Together, the excess charges on both sides are referred to as the electric double layer (EDL) (**Figure 2.4**). By applying an external electric field, the EDL can be strengthened or reversed, as desired.[25]

Various models of EDLs have emerged; the three initial models differ in how the electrolyte side is defined: the Helmholtz-Perrin model views it as a corresponding plane of positive charges, the Gouy-Chapman model rather views it as a diffuse layer, and the Stern model combines the previous two models into one. Built upon the Stern model, which does not account for electrolyte composition, is the Grahame model, which was further developed in the Bockris-Devanthan-Müllen (BDM) model, accounting for specific absorption at the electrode, so that the EDL is divided into three parts (**Figure 2.4**): from the electrode to the centre of the absorbed ions is the inner-Helmholtz plane (IHP), from the centre of absorbed ions to the centre of the first solvated ions is the outer-Helmholtz plane (OHP), and beyond that the diffusive layer.[25]

Which model is more accurate depends on the electrolyte composition,[25] which varies significantly depending on whether it is mono- or multivalent, such as a Ca-conducting. Typical monovalent electrolytes have concentrations of ~1 M,[35] while typical multivalent electrolytes are ~0.5 M.[36] As concentration increases in multivalent electrolytes, positively charged contact ion pairs (see section **3.1**) form and preferentially adsorb together onto the IHP, forming passivation layers at the electrode surface.[37] This means that the formation and the potential beneficial phases change depending on mono- and multivalent electrolytes as well.

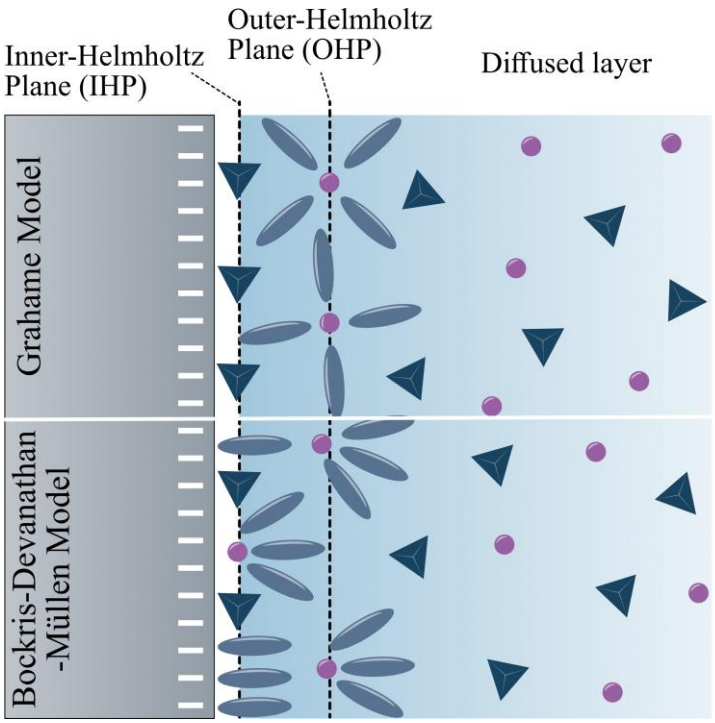

Figure 2.4 The EDL as defined by the Grahame and the Bockris-Devanthan-Müllen models.

2.4.2 Interphase formation

The demand for high-performant batteries has pushed electrode voltages to extremes, forcing the electrolyte beyond its thermodynamic limit. In doing so, the electrolyte decomposes, and the products form a new layer on the electrode surface, *e.g.*, an interphase.[34] With the discovery of the LIB, it has been found that this layer is an essential component behind its success. The name solid electrolyte interphase (SEI) was coined,[38] and as the name suggest the layer should act as a second electrolyte; isolating to electrons and conductive to ions, and separating the bulk electrode from the bulk electrolyte (**Figure 2.3**). The interphase at the cathode is called cathode electrolyte interphase (CEI). The Butler-Volmer equation (**Eq. 2.8**) now becomes invalid, and likewise the Grahame and BDM models no longer hold true, as the ions must migrate across the interphase as well (**Figure 2.5**).

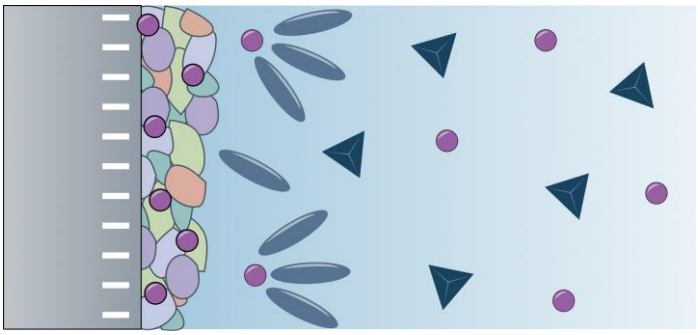

Figure 2.5 Ion migration across the SEI.

The products formed on each side are determined by the most vulnerable species in the electrolyte, which may not be the same,[34] but together they set the oxidation and reduction limits. In more detail, the thermodynamic limit of the electrolyte (**Figure 2.6**) can be defined as the electrolyte reduction at negative potentials ($-e[E_{red}]$), and the potential of solvent oxidation at positive potentials ($-e[E_{ox}]$),[39] which are dependent on the concentration of redox active species.[40] The oxidation and reduction limits are called the electrolyte's electrochemical stability window (ESW), and the main purpose of the SEI and the CEI is to extend it, so that the total potential of the cell ($e[E_{cell}]$) is extended.

As the electrolyte operates outside its thermodynamic limit, it is important that the SEI (and CEI) is stable enough to withstand the high voltage applied and remain functional. It should not be too thick, as it will hinder migration through the layer and thus be essentially isolating, but it also cannot be too thin, as it then will not prevent electron transfer. A typical SEI has been found to be around 2-50 nm,[41] but thickness, morphology, and beneficial products vary with the electrode. The SEI products should also not dissolve back into the electrolyte, as doing so would cause further electrolyte decomposition. This is particularly true for higher temperatures, as such increases the likelihood of dissolution. During charge and discharge, volume expansion and contraction occur, making good adhesion, mechanical strength, and flexibility important as well.

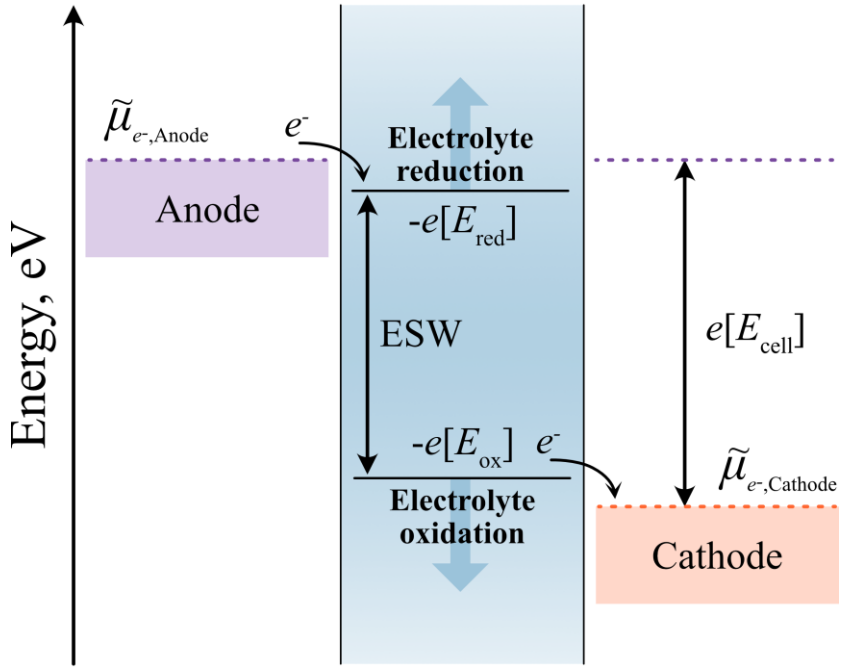

Figure 2.6 The electrolyte electrochemical stability window (ESW).

The most common SEI products for Li, Na, K, Mg, and Ca are inorganic species, typically oxides and fluorides, distributed among an amorphous mosaic structure.[27] While both mono- and multivalent batteries ideally should yield thin, homogeneous SEI layers, they differ in the proportions of inorganic and organic species, considered advantages and disadvantages.[27] In the much more well-studied LIBs, a LiF-rich SEI has been shown to be beneficial for long-term cycling.[27] CMBs, which are still in their infancy, have produced

conflicting results, suggesting what has been learnt from SEI studies of LIBs is not transferable. In general, organoboron-rich and CaF_2-poor SEIs are considered more beneficial, as passivation is avoided.[10] However, contradicting this, a CaF_2-rich mosaic interphase has also shown fast ion conduction.[42] Initial studies of bromides, iodides, and hydrides show promising results as well,[27,43,44] indicating that it is still too early to draw clear conclusions about suitable SEI layers for CMBs.

Chapter 3

Electrolytes

Rub salt in a wound: Making an already bad or painful situation worse

No other battery component is as vital to the Ca metal surface as the electrolyte, as it is the only active component that comes into direct contact with its surface. Therefore, it is crucial to understand the electrolyte structure and transport phenomena. Otherwise, the risk of *rubbing salt in a wound*, *e.g.*, introducing species that enhance the Ca metal's propensity to form passivation layers, reaches a critical height. Yet, for that sake, it should not dampen the creativity of electrolyte designs – rather the opposite. LIB electrolyte know-how is useful but not always transferable, which means functional electrolytes for CMBs must forge new ways forward. As seen in **Chapter 2**, mass-transfer is vital for the charge transfer across the interface, which is also affected by the interphase. This is controlled by the electrolyte's ability to transport ions between the electrodes. The choice and concentration of salt(s) is of utmost importance, just as the choice of solvent or lack thereof. In this chapter, the properties of liquid electrolytes and MSEs are presented, along with current trends and design principles.

3.1 Electrolyte structure

An ideal electrolyte is dilute enough so that the solvated ions do not feel the electric field of other ions. For such an electrolyte, the cation is regarded to have two solvation shells (**Figure 3.1**): the primary solvation shell, where the central cation is directly associated by strong Coulombic interactions with the solvent molecules, and the secondary solvation shell, where the solvent molecules will feel the cation's electric field, but without the strong association. The ions are in constant movement; as such, the molecules will continuously change places with each other, but on a timescale of picoseconds (10^{-12} s), molecules will always occupy the shells, in such a way that the molecules in the primary shell move together with the central cation, and the molecules in the secondary shell are oriented towards it. Outside these regions, the bulk solvent does not feel the cations' electric field.[45] Anions, which are larger and have more delocalized charge compared to cations, bond weakly to solvent molecules, making their solvation shells diffuse and less easily defined.[46,47]

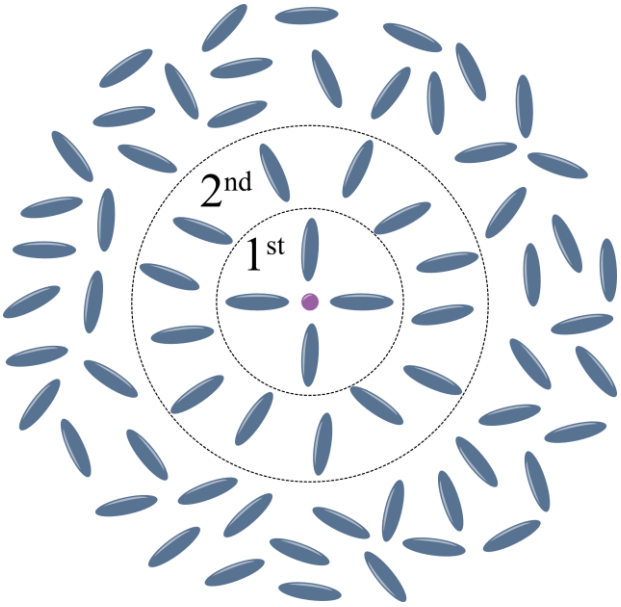

Figure 3.1 Solvent molecules structured in the primary and secondary solvation shells around a central cation.

This type of ideal electrolyte is, however, far too dilute to provide sufficient ion transport. A typical LIB electrolyte concentration is ~1 M,[35] about twice the concentration considered for liquid electrolytes developed for multivalent batteries.[36] In recent years, highly concentrated electrolytes (HCEs) (>2 M) and even super-concentrated electrolytes (>5 M) have gained research interest,[48] which has slowly started to bridge the definitions between liquid electrolytes and MSEs (**Figure 3. 2a**). While the interactions between ions and solvents were negligible in the dilute state, as the concentration starts to increase, the number of free solvent molecules in the bulk is reduced, so that occasions where the ions feel each other's Coulombic effect arise. Thus, ion-solvent interactions must be considered, which are referred to as solvent-separated ion pairs (SSIPs) and, at times, divided into solvent-shared (1SPs) and solvent-separated ion pairs (2SPs), with one or more solvent molecules between the associated ions (**Figure 3. 2bc**).

At even higher concentrations, contact ion pairs (CIPs) start to form (**Figure 3. 2d**). In these ion-ion interactions, the ions lose their individual electric fields and become charge-neutral. In the super-concentrated regime, aggregates (AGGs) of cations and anions may form (**Figure 3. 2e**).[49] Eventually, the concentration reaches the completely solvent-free region, MSEs, where, instead of solvent molecules, external heating collapses the lattice and dissociates the ions. At the same time, all ions are within close distance to each other. MSEs maintain distinct ion-order arrangements, distinguishable from those of solid salt crystals; their local structure is ordered in the short range but disordered in the long range.

The appeal of increased concentration lies in the new, often unpredictable properties it generates. Many properties are also not only a function of concentration, but rather depend on ion size, charge (monovalent or multivalent), fluorination, and other factors. Ion-ion and ion-solvation interactions within an electrolyte also depend on the combination of salt and solvent, as preferences will occur, creating an internal competition. Some cations prefer to bond more strongly to anions, making CIPs more probable, while others bond more strongly to solvent molecules, increasing the formation of SSIPs.

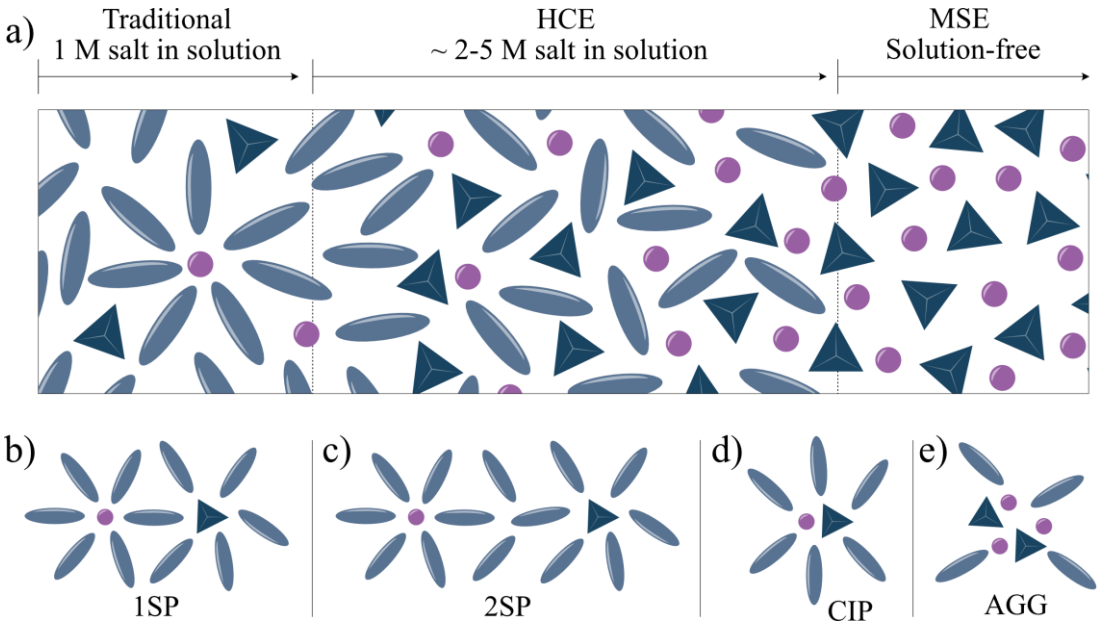

Figure 3. 2 a) Local electrolyte structure as a function of salt concentration, b) solvent-shared ion pairs (1SPs), c) solvent-separated ion pairs (2SPs), d) contact ion pairs (CIPs), and e) aggregates (AGGs).

3.2 Transport phenomena

There are three types of motion of ions in a solvent: diffusion, migration, and convection. Convection is the movement caused by hydrodynamic flow, such as stirring or shaking, and is often neglected in battery electrolytes. The other two are of great importance and closely interconnected. Diffusion describes how ions move on their own, driven by a local uneven distribution of ions, which varies over time (**Figure 3.3a**). When an external circuit is turned on, the potential difference created between the electrodes causes ions to move in a preferred direction according to the applied charge, e.g., by migration (**Figure 3.3b**). Simultaneously, the external circuit will break the previously established equilibrium at the electrode-electrolyte interface, creating a new ion concentration gradient that drive ion movement by diffusion.

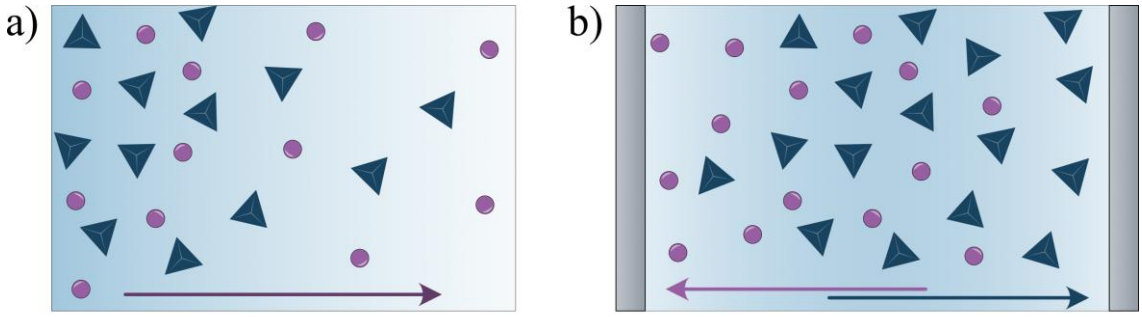

Figure 3.3 Movement of ions by a) diffusion and b) migration.

The combined diffusion and migration of ions describe ion mobility in a solvent, which further depends on the relationship between conductivity and viscosity. This can be proven

by the Einstein relation, in which diffusion in a system happens regardless of charge state,[50] so that,

$$D = \mu k_B T \tag{3.1}$$

where μ is the mobility, and k_B is the Boltzmann constant. This relation shows that diffusivity is directly correlated with ion mobility. Combining Einstein's relation with Stokes's law, which describes the drag force that acts upon a spherical object, gives the Stokes-Einstein relation,[50]

$$D = \frac{k_B T}{6\pi\eta r} \tag{3.2}$$

where η is the dynamic viscosity and r is the radius of the particle. This relation describes the diffusion of ions in a solvent. Furthermore, the diffusivity can also be understood through the conductivity, by the Nernst-Einstein relation,[50]

$$\Lambda = \frac{z_i e_0 F}{k_B T}(D_+ + D_-) = \frac{z_i F^2}{RT}(D_+ + D_-) \tag{3.3}$$

where Λ is the molar conductivity and z_i is the valence of the ions. The molar conductivity, as opposed to the ionic conductivity, considers the concentration of the electrolyte. Typically, ionic conductivity increases with salt concentration until a maximum is reached; beyond this point, the ion mobility is hindered by increased viscosity, and the ionic conductivity consequently decreases. In **Eq. 3.3**, however, the independent contributions of the diffusivity from the anion and the cation are related to the conductivity, and as such, the relation only holds true for very dilute electrolytes where no CIPs are present. For moderately concentrated electrolytes, in can be assumed that most ions are fully dissociated, though it is still enough for them to feel each other's Coulombic effect.[51] For higher concentrations, and for MSEs, which do have formation of CIPs, a correction term for **Eq. 3.3** must be added,[50]

$$\Lambda = \frac{zF^2}{RT}(D_+ + D_-) - \frac{zF^2}{RT} D_{ion\ pair} \tag{3.4}$$

It has been suggested that, despite MSEs having no solvent molecules, and thus no liquid for the ions to diffuse through, **Eq. 3.2** still holds to a rough approximation. This is related to the "voids" created in the MSEs due to the volume expansion (~10-20%) upon melting, which creates an uneven distribution over the long range, allowing ions to move. As the voids and the ions are roughly the same size, no other consideration should be needed. However, in the short range, MSEs are still ordered; thus, the correction term is added to **Eq. 3.4**.

This simplification has been disputed, as it still assumes only simple CIP formation and disregards AGGs. When AGGs are formed in complicated clusters, the overall charge might be either positive or negative, making it unpredictable to know if the overall cluster is drifting in the "right" or "wrong" direction.[52] In a multi-cationic system (see **3.4.2**) of Li bis(trifluoromethylsulfonyl)imide (LiTFSI) in an ionic liquid, it was shown that negatively charged Li^+-clusters drifted to the negative electrode due to a concentration gradient of Li^+ buildup at the interface.[52] In a multi-anionic system of Li^+ and several inorganic anions, the

lightest of the anions will drift together with the cation towards the negatively charged electrode, the anion that bonds the weakest to the cation drifts towards the positively charged electrode, and the intermediate anions might move in any direction.[53] Both these cases deal with Li^+ – a small, monovalent cation – whereas Ca^{2+}, due to its multivalent charge, may exhibit behavior different from that of Li^+.

The general assumption that increasing absolute temperature increases ionic conductivity has also been challenged for MSEs, as there is a trade-off between ion mobility and number density.[53] When the temperature increases, ion mobility increases, but the number density decreases. By keeping the temperature constant and changing the composition away from the eutectic point (see **3.4.1**), the number density could be increased, and despite lowering the ion mobility, it was effective for the overall ionic conductivity.

3.3 Liquid electrolytes

The first electrolytes for CMBs, developed in the 90's, were designed analogously to those for LIBs at the time. Thus, the salts $Ca(ClO_4)_2$ and $Ca(BF_4)_2$, were dissolved in several organic solvents, including acetonitrile (ACN), tetrahydrofuran (THF), γ-butyrolactone (BL), acetonitrile (ACN), and propylene carbonate (PC). From their electrochemical behavior, it was concluded that Ca plating and stripping were essentially impossible.[1] Not until 2016, when $Ca(BF_4)_2$ was dissolved into a mixture of ethylene carbonate (EC) and PC at 100 °C, was reversible plating and stripping achieved.[2] Since then, several electrolyte concepts have emerged, three of which will be focused on in this thesis: (i) boron-based electrolytes, (ii) high donor number (DN) solvents, and (iii) introducing alkali salts into the electrolyte as a primary or co-salt.

The $Ca(BF_4)_2$ in EC:PC electrolyte, which greatly benefited from elevated temperature by hindering the formation of passivation layers, sparked a search within the community for electrolytes that worked at room temperature. The first to be successful was $Ca(BH_4)_2$ in THF.[26] Based on these initial findings, boron emerged as a recurring design principle for enabling Ca electrochemistry. However, $Ca(BF_4)_2$ struggles with water contamination originating from its synthesis[54] and $Ca(BH_4)_2$ suffers from low oxidative stability. This increased the desire for new boron-containing Ca-salts – a gap which was eventually filled by $Ca[B(hfip)_4)]_2$.[55,56] With demonstrated reversibility in numerous solvents,[57,58] it is arguably the most successful boron-based concept so far. It is, however, not a commercial salt, making it difficult to use as a common basis for CMB development.

Commercially readily available Ca-salts, such as $Ca(TFSI)_2$, were eventually found to work with the support of strongly solvating, high DN solvents, such as trimethyl phosphate (TMP), triethyl phosphate (TEP), dimethylformamide (DMF), 1-methylimidazole (MeIm), and dimethylacetamide (DMAc).[12] The combination of strongly solvating solvents and highly dissociated salts led to solvent-dominated solvation shells. Compared to low-DN solvent electrolytes with similar ionic conductivities, high-DN solvent electrolytes formed preferential solvation structures at the electrode/electrolyte interface.[12] Building from this, similar concepts have been extended to dimethyl sulfoxide (DMSO) containing formulations.[42] Other salts, such as Ca triflate ($Ca(OTf)_2$) and Ca bis(fluorosulfonyl)imide ($Ca(FSI)_2$), have also been tried, but were found to be more challenging to dissociate

compared to $Ca(TFSI)_2$, though not impossible, as $Ca(OTf)_2$ was found to enable stable cycling under diverse and challenging conditions in NMA:TMP mixtures.[33]

While the boron-based concept plays with the anion chemistry and high-DN solvents play with the solvent chemistry, the final concept presented here plays with the cation chemistry. The strong Coulombic interactions from the Ca^{2+} cation can be disrupted by introducing other cations, such as Li^+ or Na^+.[59–62] Doing so has shown to improve desolvation and charge transfer[60,63] and simultaneously reduce ion-pair formation, thereby increasing cation accessibility and mobility.[63,64] To date, most dual-salt work has focused on Li and Na salts,[59–62] but K-salt has also been proposed to enable Ca metal cycling as well.[65] The main benefit was attributed to the creation of a hybrid SEI, composed of both Ca-rich species and K-derived inorganic compounds,[65] the latter analogous to those found using Li-[62] and Na-based[61,66] electrolytes. This even when Ca salts are not initially present.

For the work on which this thesis is based, various salts and solvents have been used. In **Paper IV**, the variable quality of five commercially sourced $Ca(FSI)_2$ salts was assessed by dissolving them in the high-DN solvent DMAc. In **Paper III**, the boron-based anion, BF_4^-, and the low-DN anion, OTf^- (**Figure 3.4**), were similarly dissolved in another high-DN solvent, DMSO, both with their Ca salt and K salt counterparts, and a combination of both.

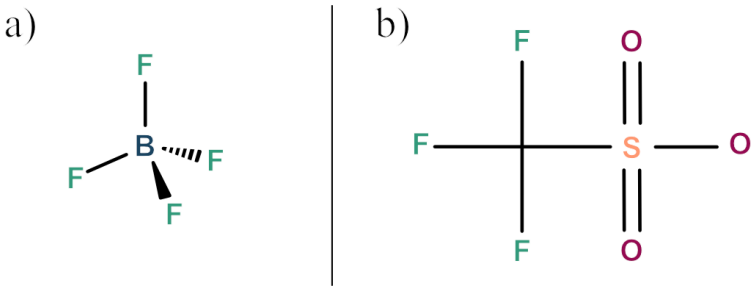

Figure 3.4 Chemical structure of BF_4^- and b) OTf^-.

3.4 Molten salt electrolytes (MSEs)

MSEs and ionic liquids consist solely of ions and have no molecular species, and by this definition can be considered the same thing. Traditionally, they go by different names because they were developed in parallel by research groups unaware of each other's work.[67] As a consequence of this shared history, they are commonly categorized by temperature: salts that melt below 100 °C are called ionic liquids, and those that melt above 100 °C are called molten salts.[68] The definition used in this thesis, however, categorizes them by ion *type*. The cations in MSE are typically inorganic, such as Li^+, Na^+, K^+, and Ca^{2+}, whereas those in ionic liquids are large and organic (**Figure 3.5**). The large organic cations in ionic liquids help lower the salts' T_m to room temperature or lower.[69] Meanwhile, MSEs typically exist in binary or higher-order systems to reach lower T_m.[69] Yet, any single salt whose cations and anion can be dissociated by temperature can become a molten salt.[48]

Systems of MSEs have been tested in different chemistries, from traditional LIBs[70] to NGB concepts such as lithium-air,[71] Na-ion[70] and Na-metal,[72,73] and Al-ion[74] and Al-metal batteries.[75] Frequently, these MSEs consist of different chloride salts, some with high melting points of around 350-500 °C,[72,73] others have successfully made use of $AlCl_3$,

which forms large Al_xCl_{3x+1}–moieties, which brings down the melting temperature to 120 °C[74] or even 93 °C.[75] Combinations of binary and ternary mixtures of either TFSI,[76–78] FSI,[79–83] or (fluorosulfonyl)-(trifluoromethane-sulfonyl)imide (FTFSI)[84–88] have also been explored, there it is shown that it is possible to bring down the melting temperature to as low as 36 °C, still only using inorganic cations.

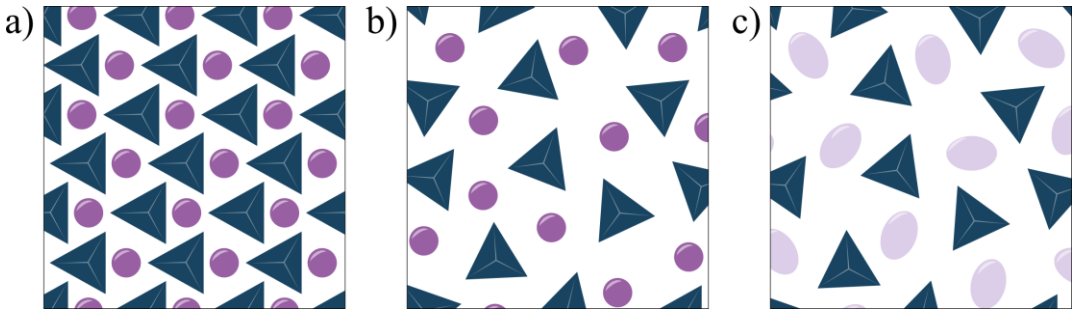

Figure 3.5 Visualization of a) a single salt, b) a molten salt, and c) an ionic liquid.

MSEs for CMBs have so far been scarcely explored,[89–91] particularly for rechargeable batteries in the 80-120 °C temperature range. This temperature region has gained interest for batteries related to appliances that generate significant internal heat during operation, such as in electric vehicles (EVs) and grid energy storage, but in particular those naturally operating at high temperature in more extreme environments, such as in desert climates and for space exploration.[7,8] MSEs, which are naturally solvent-free, are far safer than liquid electrolytes for these applications, as they pose no risk of ignition/flammability or of vapor pressure buildup from organic components.

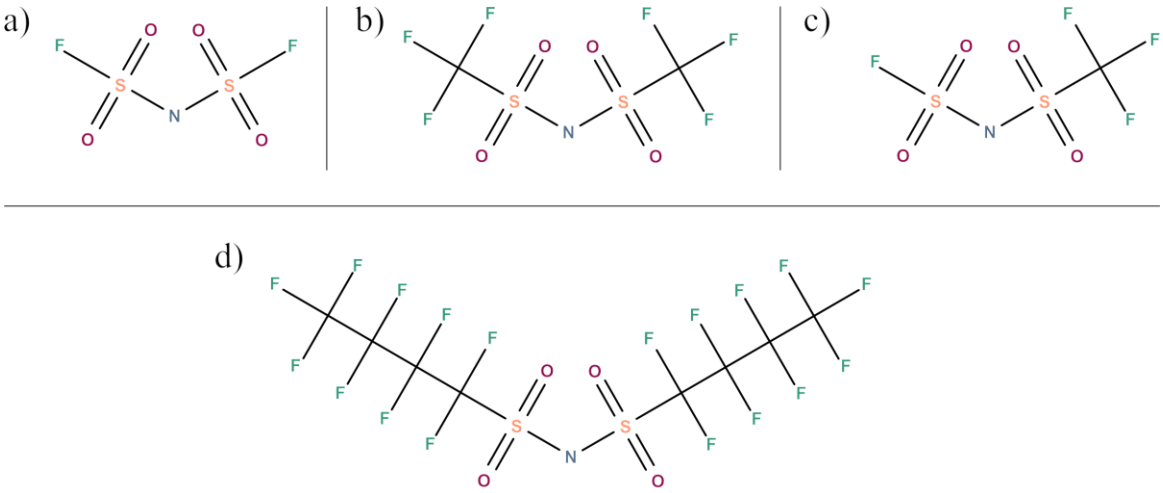

Figure 3.6 Chemical structures of a) FSI, b) TFSI, c) FTFSI, and d) NFSI.

The MSEs presented in this thesis belong to the low-melting salts of the FSI/TFSI/FTFSI family (**Figure 3.6a-c**), foremost in combination with Ca^{2+}, but also together with Li^+, Na^+, K^+, and Cs^+. They are structurally very similar; they are large, which delocalizes the negative charge and reduces the Coulombic field, and are commonly used in batteries for their chemical and thermal stability.[92] With nitrogen at the center, with two "wings" containing the other elements, only the fluorine content differentiates them. The FSI anion

has the least amount of fluor, and TFSI has the highest, while FTFSI has one “wing” from each. The asymmetry of the FTFSI-salts makes them particularly low-melting. In two instances in **5.1**, the anion bis(nonafluorobutanesulfonyl)imide (NFSI) has also been used, which is substantially fluorinated (**Figure 3.6d**). Building from this family of salts, two general design rules have been accounted for in this thesis: (i) lowering of the melting temperature (**3.4.1**), and (ii) formation of homogenous mixtures (**3.4.2**).

3.4.1 High entropy electrolytes

The interest in intentionally increasing a system's entropy stems from high entropy alloys (HEA),[93] which, by definition, combine five or more components, creating properties far superior to those of lower entropy.[94] In recent years, the interest has expanded to other types of materials, such as ceramics[95] and for specific applications, such as energy storage.[96] In terms of electrolytes, some refer to having high entropy electrolytes by using several solutions,[97,98] others do so by using more than one salt,[99] and others do both.[100] By using more than one solvent, the cation mobility was increased[97] and hence led to higher diffusivity and conductivity. This was shown to be due to a smaller cationic clustering.[101] Furthermore, increased entropy lowered the electrolyte's freezing temperature and increased the battery cell's operating temperature.[97]

MSEs have a natural history of increased entropy, as they are typically combined in binary or higher-order electrolyte as a design consideration to lower melting temperatures. This can be demonstrated by a simple binary phase diagram at constant pressure (**Figure 3.7**). When two components, A and B, each with high melting temperatures, are gradually combined, a point will be reached at which the composition of both will go directly from solid to liquid at a much lower melting point. This is the eutectic point. At all other compositions of A and B, the eutectic composition, together with either solid A or B, exists. Phase diagrams of ternary, quaternary, or higher-order electrolytes are possible, but are experimentally very time-consuming.

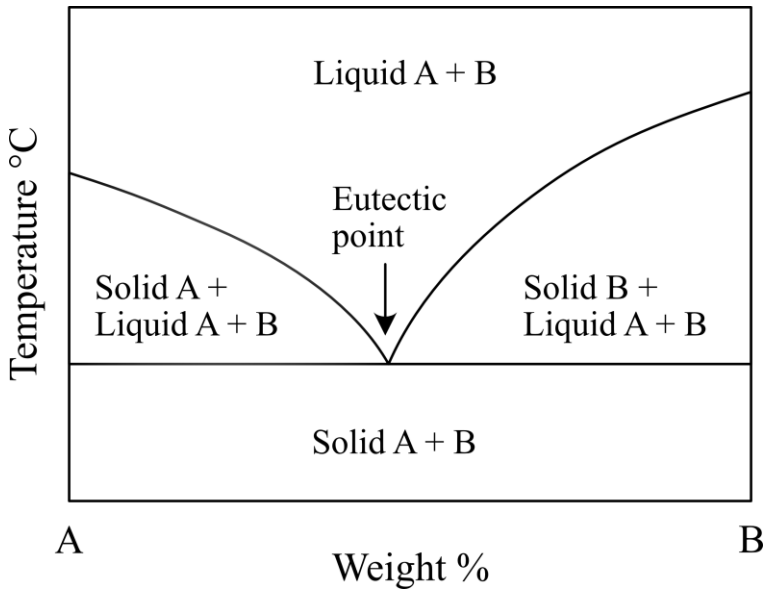

Figure 3.7 Binary temperature-composition phase diagram of components A and B, at constant pressure.

The reason behind the lowered melting point can be explained by the change in Gibbs free energy (ΔG) at a constant temperature, T, written as,

$$\Delta G = \Delta H - T\Delta S \tag{3.5}$$

where ΔH is the change in enthalpy and ΔS is the change in entropy of the system. For a pure system, like a single salt, which goes through a phase change, the corresponding equation is,

$$\Delta G_{fus} = \Delta H_{fus} - T\Delta S_{fus} \tag{3.6}$$

For compositions, whether binary or higher order, such as MSEs, there is a contribution from both fusion and mixing. Here, only the mixing effect is assumed,

$$\Delta G_{mix} = \Delta H_{mix} - T\Delta S_{mix} \tag{3.7}$$

where the entropy of mixing is given by

$$\Delta S_{mix} = -nR \sum_i x_i \ln x_i \tag{3.8}$$

where n is the total number of moles and x_i is the molar fraction of the species i. Because $\ln x < 0$, it follows that $\Delta S_{mix} > 0$ for all compositions. Consequently, adding multiple components to increase ΔS serves as a tactic to counterbalance ΔH, thereby decreasing the free energy. While enhancing the entropy of MSEs is powerful for lowering the operating temperature, the eutectic composition is not necessary for the best overall conductivity,[53] as seen in **3.2**.

3.4.2 Multi-anionic and multi-cationic MSEs

MSEs can be created with various degrees of complexity, typically limited by the enthalpy of mixing, which determines whether a combination of salts forms a homogeneous mixture.[102] Keeping this in mind, two things need to be considered: (i) if the salts contain a common cation (anion) combined with multiple anions (cation) and therefore is multi-anionic (multi-cationic) (**Figure 3.8ab**) or contain a mixture of both different cations and anions (**Figure 3.8c**), and (ii) if all cations in the MSE have the same charge (only monovalent or only multivalent) or different charges (monovalent together with multivalent). In the least complex case, where either multi-anionic or multi-cationic MSEs have the same charge, the change in enthalpy is related to the ionic radius.[103] Multi-cationic MSEs, in general, have a more ideal enthalpy of mixing when the species are not too different in size. When comparing multi-cationic mixtures of analogous anions, the variation in the enthalpy of mixing is small. For analogous multi-anionic electrolytes, the same is true if the relative anion size difference is small. If not, the larger the difference between the anions, the more endothermic the enthalpy of mixing.[102]

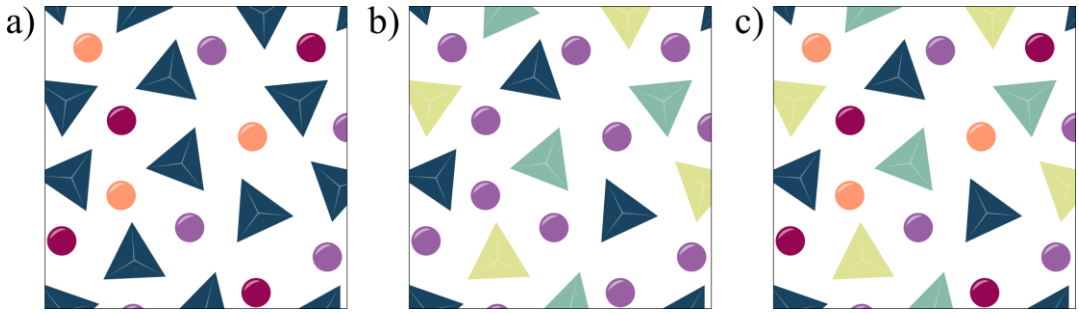

Figure 3.8 MSE of a) multi-cationic, b) multi-anionic, and c) mixed cations and anions.

Increasing the level of complexity to multi-cationic MSEs with different charges has been shown to create a “competition" between the cations for the common anion, driven by the polarizing power of the cations. Depending on how large the competition is, the formation of complex AGGs is more or less likely to occur. Mixing multivalent cations with small cations like Li^+ and, to some extent, Na^+ results in small enthalpies of mixing, making complex AGGs less likely, whereas mixing with large cations like K^+, Rb^+, and Cs^+ results in more negative enthalpies of mixing, making them more prone to complex AGGs.[102] Complex AGGs in MSEs exhibit unpredictable behavior: while their formation can lead to inhomogeneous mixtures and be detrimental,[102] it has also been shown in other cases to drastically decrease melting temperatures.[75] Comparing multivalent cations, the larger polarizing power of Mg^{2+} relative to that of Ca^{2+} makes Mg^{2+} more prone to create complex AGGs.[102]

In the most complex case, in which both cations and anions of any charge are combined, the ideal mixing of the salts is AX+BY=AY+BX, where salt *AX*, containing cation *A* and anion *B*, is mixed with salt *BY*, containing cation *B* and anion *Y*, would create the same mixtures as combining salt *AY* and *BX*.[102] However, mixtures are often not ideal; hence, the species formed will depend on which are energetically favorable. Typically, small cations are drawn to small anions, and large cations are drawn to large anions,[104] which will create short-range ordered clusters in the melt. Regardless of the level of complexity of MSEs, the salt choices need to be carefully considered.

Chapter 4

Experimental techniques

Back to the salt mines: Return to hard and tedious work

The backbone of this thesis lies in the numerous salts that have been thoroughly dried, carefully weighed, and with precision ground to MSEs or dissolved to liquid electrolytes. And in the plentiful vials, neatly labeled, containing electrolytes whose structures have been studied. And in the Ca metal electrodes, which had their passivation layers thoroughly polished off, and have been assembled into countless coin cells. Yet, this chapter will focus solely on the experimental techniques used and their theoretical background, with all specific experimental details left for the respective **Papers I-V**.

4.1 Physical characterization

This section is divided into three parts. The first two present physical characterization techniques – thermal gravimetric analysis (TGA) and differential scanning calorimetry (DSC) – essential for characterizing the degradation and phase transitions of pure salts, as well as for initial evaluation of MSEs. The third part describes measuring ionic conductivity in liquid electrolytes using an ionic conductivity meter.

4.1.1 Thermal gravimetric analysis

With TGA, the mass change in a material is measured under a controlled temperature program, either continuously increasing (dynamic) or held at a constant temperature (isothermal).[105] This way, it is possible to determine at what temperature or at what time a material starts to decompose, resulting in a characteristic step curve (**Figure 4.1**). While some materials might only decompose in one step, several steps are also possible. Most commonly, the 1% and 5% of mass loss are examined, referred to as $T_{d1\%}$ and $T_{d5\%}$, respectively. For very pure materials, $T_{d1\%}$ provides a good indication of the onset of decomposition. However, if impurities are present, the onset might start earlier, falsely showing material breakdown before the main decay, leading to deceptive results. Hence, $T_{d5\%}$ provides a good addition in combination with $T_{d1\%}$.

In the work this thesis is based on, $T_{d1\%}$ and $T_{d5\%}$ have primarily been used as initial judgments of suitable single salts for MSEs and of the MSEs themselves, as seen in **Paper I** and the unpublished results in section **5.1**. The MSEs were tested in their powder form, directly from the preparation step, but as they melt far before they decompose, accurate decomposition temperatures are still provided. Decomposition temperature and time were

also studied in **Paper IV**, where impurities and structural differences in $Ca(FSI)_2$ salts from different suppliers were assessed.

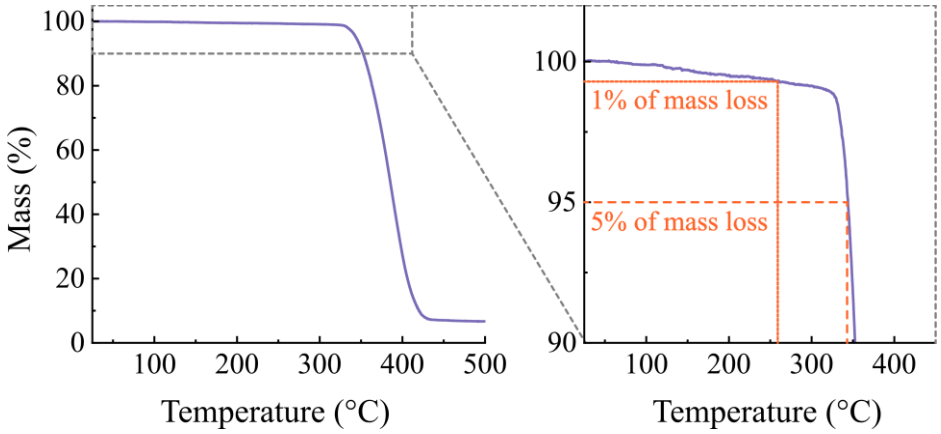

Figure 4.1 Dynamic TGA trace showing overall behaviour and close-up of the 1% and 5% mass losses.

4.1.2 Differential scanning calorimetry

In DSC, a hermetically sealed pan containing the sample to be studied and an empty pan serving as a reference are placed on their respective sample holders in the same furnace.[106] The pans go through a pre-decided programme of heating and/or cooling, during which the heat fluxes to the sample and the reference are to be kept even. Any deviation will create a peak in the thermal analysis curve (**Figure 4.2a**), where an endothermic reaction most typically indicates melting and an exothermic reaction typically indicates crystallization. The temperatures at the onset of melting and crystallization are denoted T_m and T_c, respectively. With the same temperature program, DSC provides high accuracy; properties such as T_m and T_c should therefore be consistent for the same salt from different suppliers. For the five commercial $Ca(FSI)_2$ salts in **Paper IV**, DSC was instrumental in detecting the potential impurities and structural differences.

Reaching a low T_m was of particular importance when choosing single salts for low melting ternary and quaternary MSEs in **Paper I**. Also reported there was the glass transitions, T_g, which appears as a step in the thermal analysis curve (**Figure 4.2b**), due to no formal phase change occurring, but rather a phase relaxation. As such, neither the onset nor endpoint of the transition, but instead the temperature at midpoint, is used to define the T_g. In this thesis and the corresponding papers, the T_m reported for the MSEs is determined by the initial heating of crystalline powders. This, as already molten MSEs, when cooled and reheated, will only exhibit a glass transition – pointing to inherent slow dynamics and non-equilibrium. The T_m and T_g of these MSEs also played an important role in **Paper II**; the T_m determined the allowed operation temperature, and the T_g was hypothesized to affect the actual cyclability of the cells.

The area between the melting peak and the baseline in the thermal analysis curve corresponds to the enthalpy of fusion, ΔH_{fus}, for a pure material (**Figure 4.2c**). This has been used in **Paper V**, where the T_m and ΔH_{fus} were used as input values in a computational model to predict solubilities in different solvents. The same area, for MSEs, is rather

designated as the enthalpy of mixing, ΔH_{mix}, as the contribution of fusion and mixing cannot be distinguished here. The melting behaviour of MSEs, particularly in higher-order systems where ΔS_{mix} is increased, largely depends on how well the corresponding single salts mix. When they do not mix well, several melting peaks can occur (**Figure 4.2d**), which was used as a design rule for unpublished results discussed in section **5.1**.

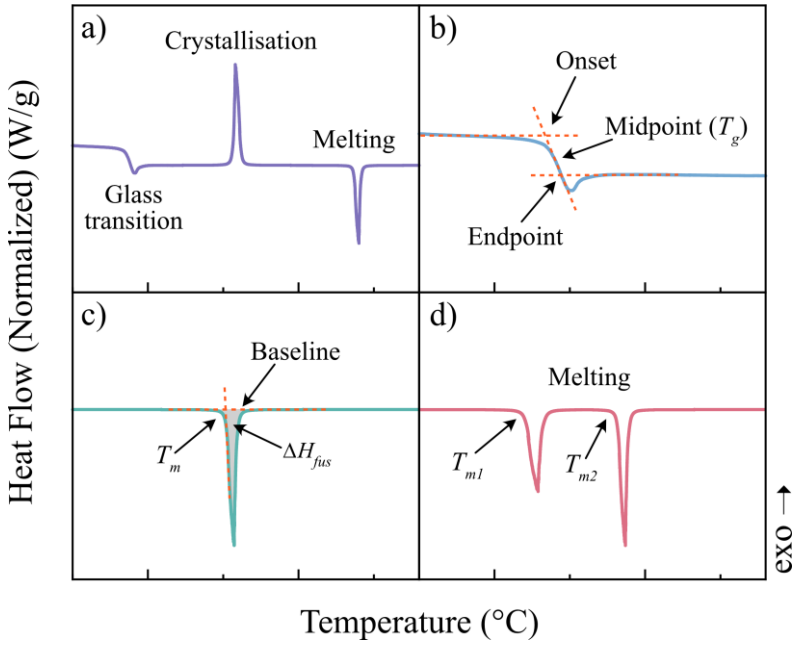

Figure 4.2 A typical DSC trace showing a) glass transition, crystallisation and melting for a single salt, b) a close-up of glass transition with onset, endpoint and midpoint, c) close-up of the melting point and the change in enthalpy, and d) melting peaks for a MSE with separate melting points.

4.1.3 Ionic conductivity

The ionic conductivity of liquid electrolytes in **Paper III**, it was measured directly using an ionic conductivity meter. The ionic conductivity meter consists of two electrode pairs: the outer electrodes, which are driven by an applied alternating current, and the inner electrodes, which are placed in the outer electric field. The current flowing through the outer electrode and the electrolyte solution is measured with a high-impedance amplifier within the inner electrodes. The conductivity can then be calculated by,

$$\sigma = \frac{1}{R} \times \frac{l}{A} = G \times K \tag{4.1}$$

where R is the resistance, l is the distance between the inner electrodes, A is the area of electrolyte between the inner electrodes, G is the conductance, and K is the cell constant.[107]

4.2 Vibrational spectroscopy

Vibrational spectroscopic techniques, such as Raman spectroscopy and Fourier-transform infrared spectroscopy (FTIR), give insight into the local structure of the materials studied. This means that characteristics such as composition, interactions, and phase can be

determined. In both techniques, light hits the sample, and the resulting interaction depends on the atom's vibrational motion. If the resulting motion changes the angle between two atomic bonds, it is called bending; if it occurs in the same direction as the atomic bonds, it is called stretching.[108] Categorizations, such as bending and stretching, are examples of different modes, as seen in **Figure 4.3**. It is also noted that symmetry is of great importance. Symmetry planes between atoms must have a well-defined relationship; depending on whether the atoms move in-phase or out-of-phase, this gives rise to symmetric or asymmetric modes, respectively.[108]

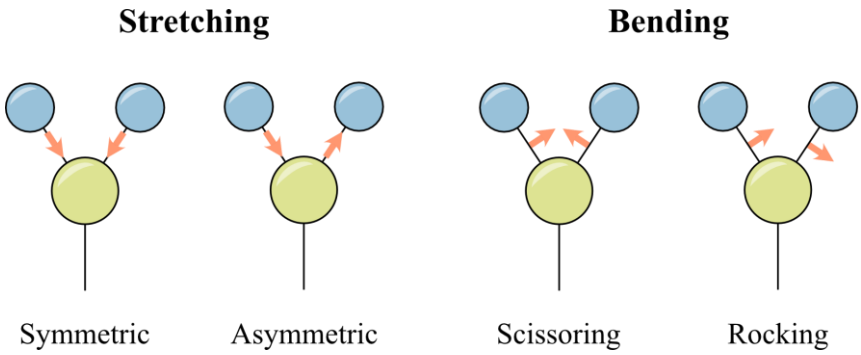

Figure 4.3 Selected vibrational motion of atoms.

Vibrational motions of atoms are not random; they can be predicted according to selection rules. However, selection rules do not specify the interaction intensity; they only indicate whether it is zero (forbidden) or nonzero (allowed). Some modes might have the same vibrational frequency, or very close to it, making the modes degenerate. Transitions appearing in Raman spectra are called Raman active, and those that appear in FTIR spectra are called FTIR active, and it all comes down to the symmetry of the molecule. This means that bands might or might not overlap, as seen by typical spectra of Raman and FTIR in **Figure 4.4**, which means that the techniques are complementary and together provide a more complete picture of a material's vibrational states.[108]

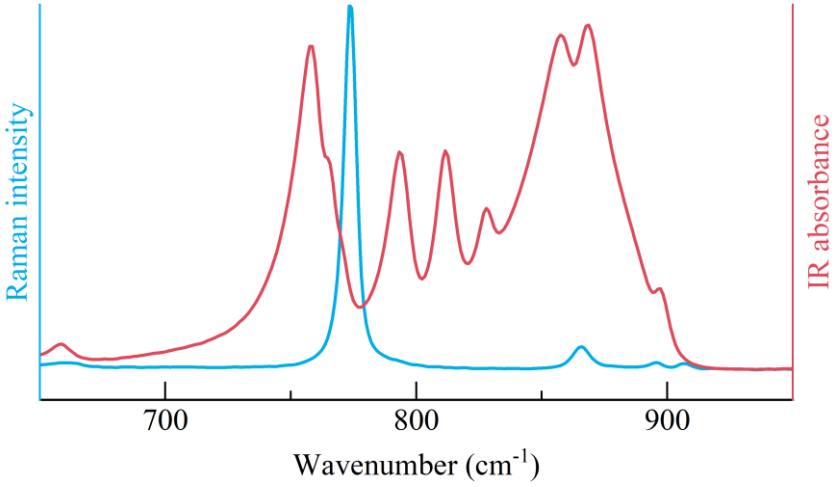

Figure 4.4 Typical differences in Raman (blue) and FTIR (red) spectra of the same material.

4.2.1 Raman spectroscopy

In Raman spectroscopy, light of a single known frequency, ν_0, impinges on the sample. Most of the light passes right through, but a small amount, roughly 1/1000 of the resulting photons scatter, and do so in all directions, either elastically or inelastically, as can be seen in **Figure 4.5**. The energy at which photons scatter depends on the atoms' vibrational motion. The photons that scatter elastically, that is, when the frequency in (v_0) and the frequency out (v_0), are the same, are called Rayleigh scattering. The photons that do not scatter with the frequency v_0 have instead scattered inelastically, which means that the material has absorbed some of the light and is therefore either greater than (Stokes) or less than (Anti-Stokes) the frequency v_0. While both Stokes and Anti-Stokes scattering are part of Raman scattering, they provide the same information; however, Stokes scattering is stronger and is therefore more commonly used.[108]

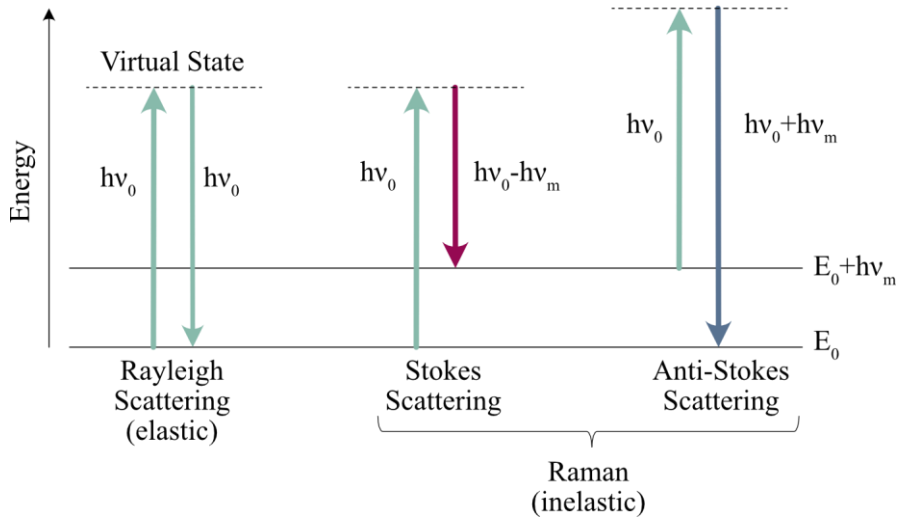

Figure 4.5 Schematic energy diagram showing the principles of elastic (Rayleigh) scattering and inelastic (Raman) scattering.

Raman spectroscopy has been used in **Paper I** to compare the local structure and ion-ion interactions of MSEs, as a function of the entropic effect at different states of ageing, in **Paper III** to look at the ion-solvent and ion-ion interactions of Ca-, K-, and mixed-salt electrolytes, and in **Paper IV** to evaluate purity of $Ca(FSI)_2$ from different suppliers. Furthermore, in section **5.2** of this thesis, the local structure of MSEs and liquid electrolytes has been compared.

4.2.2 Fourier-transform infrared spectroscopy

As opposed to Raman spectroscopy, where light of a single frequency hits the sample, in FTIR spectroscopy, light of all different frequencies is used instead. The sample absorbs frequencies that match the molecule's own frequency, while frequencies that do not match pass through the sample (**Figure 4.6**). The intensity of the transmitted light is then measured at each frequency. For absorption in the FTIR region to arise, there must be a change in the molecule's dipole moment. Because symmetric vibrations do not change the dipole moment, in-phase motion of atomic bonds is not FTIR-active.

FTIR spectroscopy has been used in the supplementary information of **Paper III** to complement the observations of ion-solvent and ion-ion interactions of the Ca-, K-, and mixed-salt electrolytes, and in **Paper IV**, for potential observation of additional bands between the compared salts' purity. These results are not commented upon in this thesis.

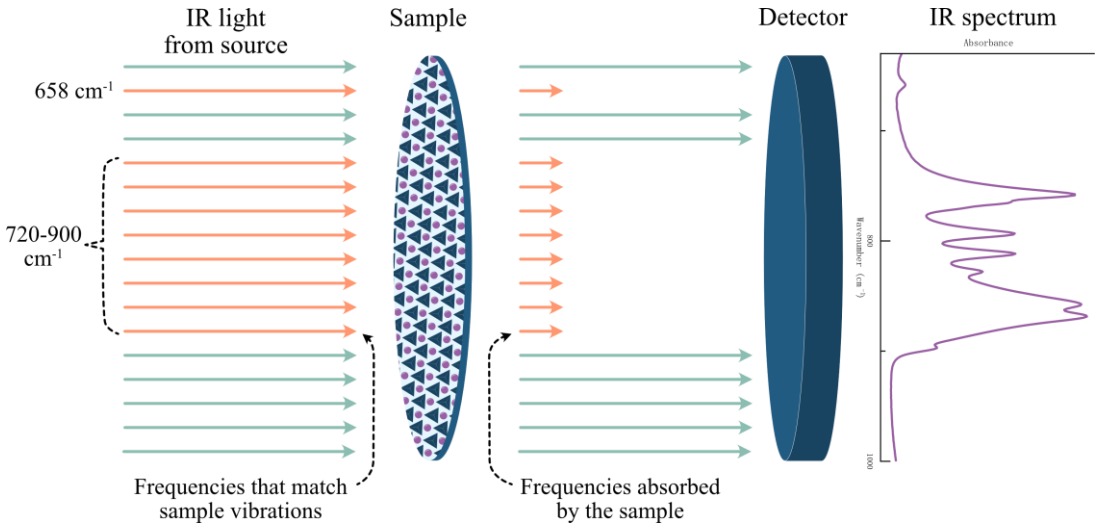

Figure 4.6 Schematic of IR light being absorbed or passed through the sample, and then caught by the detector, resulting in the characteristic FTIR spectra.

4.3 Electrochemical characterization

Battery testing is typically performed in a two-electrode configuration (**Figure 4.7a**), where current flows between the counter electrode (CE) and the working electrode (WE). Because the electrode potential can only be measured relative to another electrode, this configuration only allows measurement of the potential difference between the CE and WE. Any overlapping features, such as polarization from both, cannot be distinguished. To see the potential at the WE, a reference electrode (RE) needs to be introduced, separated from both in a three-electrode configuration (**Figure 4.7b**). The RE only has a very small current running through it, enough to measure the potential to the WE. The RE must be stable and not chemically or electrochemically react with any other cell components. In tests with Ca metal as CE/WE, a Ca metal RE should be avoided due to its reactivity; instead gold (Ag) or platinum (Pt) is often used as RE.[109]

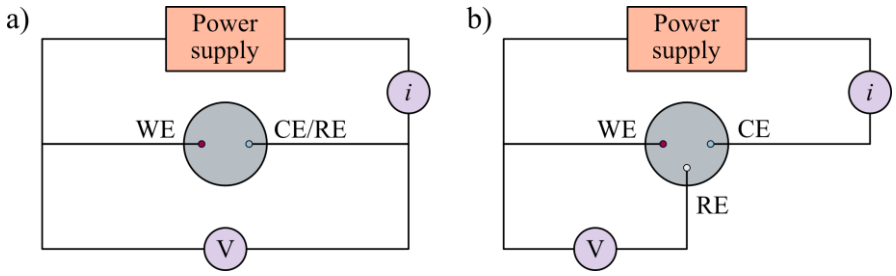

Figure 4.7 Circuit diagram showing a) two-electrode setup, and b) three-electrode setup.

Testing of the different battery materials is done in different cell configurations. Symmetric cells (**Figure 4.8a**), where both electrodes are of the same metal, in this case both Ca, are used to measure the compatibility between electrolyte and metal anode. This indicates short-circuiting or interfacial resistance during cycling. Half-cells are used to evaluate the efficiency of metal plating and stripping (**Figure 4.8b**), in which Ca metal serves as an ion reservoir (CE) together with a nonreactive metal, typically SS (WE). Full cells, in which Ca metal (CE) and a cathode material (WE) are combined (**Figure 4.8c**), are the only type that act as complete batteries, allowing evaluation of the system's overall compatibility.

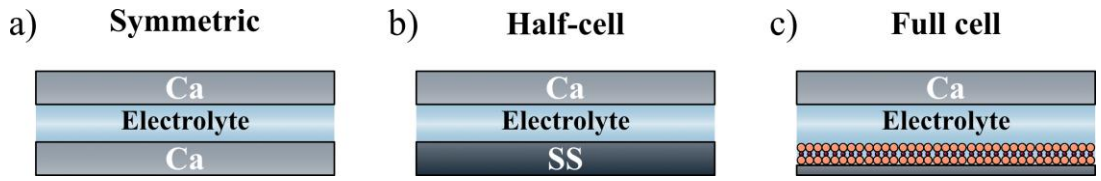

Figure 4.8 Cell configurations used for analysing electrolytes: a) symmetric cell, b) half-cell, and c) full cell.

4.3.1 Galvanostatic cycling

Galvanostatic cycling (GC) is the most widely used electrochemical method for evaluating battery materials and full cells. The current is controlled so that a fixed current flow between the CE and WE, and the potential needed to maintain it is measured.[110] The output is often displayed as voltage *vs*. capacity or as voltage *vs*. time (**Figure 4.9**). The former, used in half- and full cells, allows determination of rate capability and Coulombic efficiency within a narrow voltage window. In this thesis, the latter has mostly been used to evaluate electrolyte performance in symmetric two-electrode Ca||Ca cells. The fixed current switches from negative to positive at a set time and continues until the voltage cut-off limits (E_1 and E_2) are reached. The electrolyte potential and cycle life can this way be decided. CG tests, while less sensitive to the absence of a RE, might still shift the resulting GC curve to a lower or higher potential if passivation occurs at either electrode.[109]

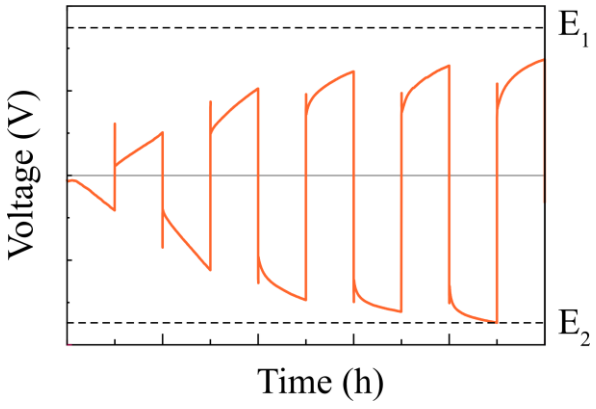

Figure 4.9 Schematic GC-curve.

4.3.2 Cyclic voltammetry

In cyclic voltammetry (CV) (**Figure 4.10**), the second most widely used electrochemical method for battery testing, the cell voltage is swept at a constant rate between two potential limits (E_1 and E_2) and the corresponding current is monitored.[111] This allows for the investigation of reduction and oxidation potentials of different reactions. When a redox reaction occurs, a characteristic peak will appear. If the reaction is reversible, the peak appears on both positive and negative sweeps; if not, the reaction is irreversible.[110] With electrolytes containing more than one charge carrier, such as in **Papers II** and **III**, multiple peaks might be present, indicating multiple redox processes. As the current varies during a CV experiment, it is more sensitive to the absence of a RE, where the shape of the curves could be substantially altered.[109]

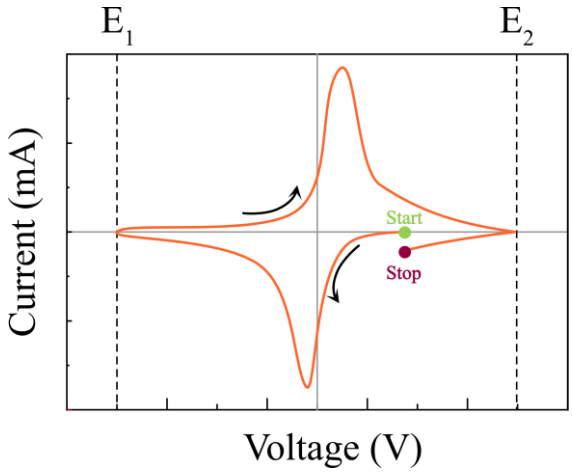

Figure 4.10 Schematic CV-curve.

Chapter 5

Results and Discussions

Take with a grain of salt: To not believe something completely, to view it with skepticism

If there is something to be learnt of the history of CMBs, it is that definite findings occasionally should be *taken with a grain of salt* – otherwise their revival never would have happened. As new reports are published, some of which contradict each other, it is important to remember that different circumstances result in different outcomes. For batteries based on Ca metal anodes, which are in their infancy, getting too stuck on one route could mean missing another. In this chapter, we will move from single salts to the formation of electrolytes and examine how their local structure affects the electrochemical performance of Ca metal anodes. All of which are affected by the initial quality of the Ca-salts employed. Connections within **Papers I-V**, alongside unpublished work, reveal what makes for a good MSE, how much development MSEs still need, to catch up with liquid electrolytes, and how alkali metal salts, as an addition or as a replacement for Ca-salts, might lead to unexpected outcomes.

5.1 Thermal properties of salts and electrolytes

Thermal properties such as melting and decomposition temperatures of salts and MSEs provide, as a first level of approximation, some insight into suitable MSE compositions. Numerous salts have been used in this thesis (**Figure 5.1a**); particularly low-melting salts of the FSI/TFSI/FTFSI family, foremost Ca, but also Li, Na, K, and even Cs. At first glance, the Ca-salts (**Figure 5.1b**) and the alkali metal salts have quite different appearances, as the Ca-salts' melting peaks are significantly less deep, indicating a less exothermic reaction. The strong Coulombic attraction between the Ca^{2+} cation and the anions makes this behaviour expected, and this also explains why the Ca-salts have much higher T_m than their analogous alkali metal salts.

Not in the same family of salts, are the salts LiC_2H_5O, NaC_2H_5O, and NaHCOO (**Figure 5.1a**). For these T_m and ΔH_{fus} have not been used as estimations of good MSE components, but rather as input for the conductor-like screening model for real solvents (COSMO-RS) modelling of SEI species solvation presented in **Paper V**. Therein, prospective SEI species in both LIBs and NGBs, have been viewed as simple salts, whose stability in the SEI depends on their solubility in common solvents. Apart from the mentioned Li- and Na-salts, most of the T_m and ΔH_{fus} values of additional Li- and Na-salts, but also Ca- and Mg-salts,

were taken from literature, and they were all used to calculate the Gibbs free energy of fusion (ΔG_{fus}) as follows,

$$\Delta G_{fus} = \Delta H_{fus}\left(1 + \frac{T}{T_m}\right) \tag{5.1}$$

where T is the temperature at which the solubility is measured.

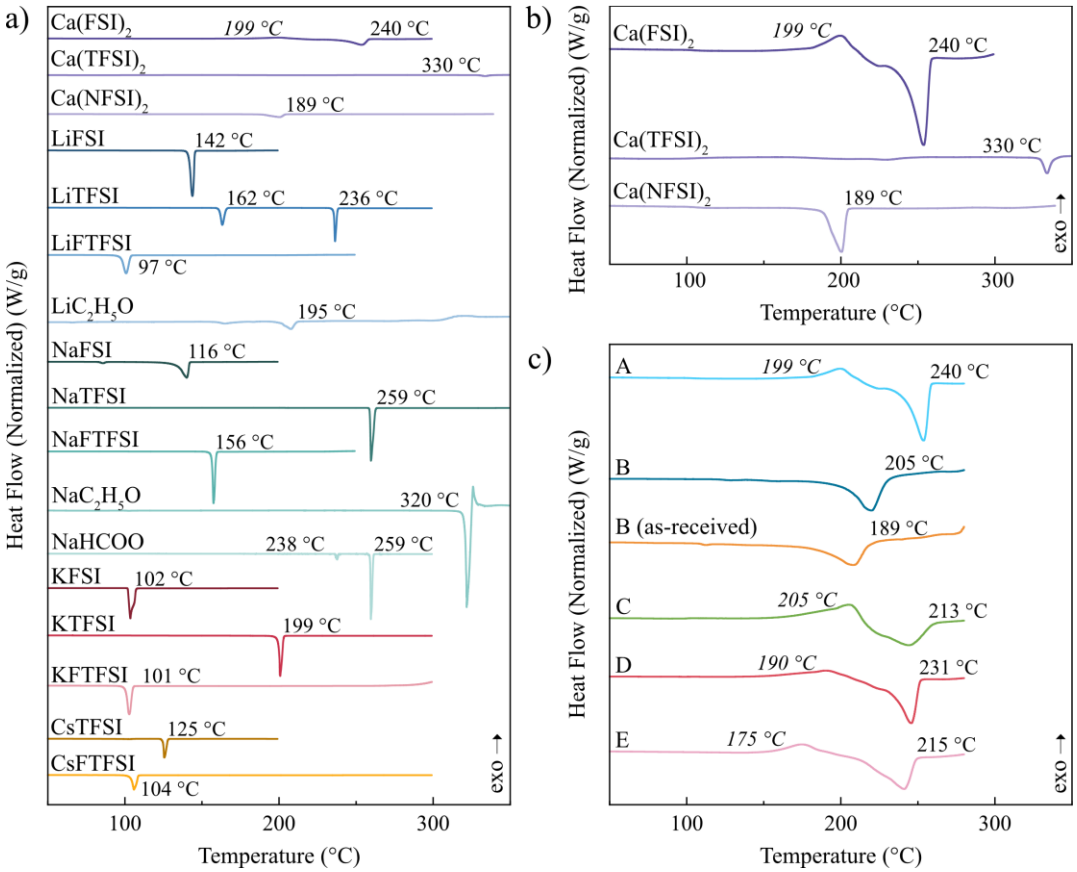

Figure 5.1 DSC heating traces and corresponding event temperatures of a) various single salts, b) close-up of Ca-salts, and c) $Ca(FSI)_2$ salts A–E.

The ability to take values from literature and experimentally complement them, very much depends on the reliability of commercial salt, as the same salt should yield the same physico-chemical properties. This is something found not always true, as shown in **Paper IV**, where $Ca(FSI)_2$ from five different suppliers A-E, were compared (**Figure 5.1c**). While salts A and C-E show exothermal events followed by the endothermic melting peak at rather similar temperatures, salt B, notably, both as-received and dried, shows no exothermic event at all and has a T_m much lower than the other salts. A more complete picture of the thermal properties is provided by considering both the dynamic and isothermal TGA traces (**Figure 5.2**). These show that salt B loses significantly more mass in both cases compared to the other salts. In the isothermal TGA, salt C also loses a considerable amount of mass.

The differences seen in salt B, both as-received and dried, and to some extent in salt C, cannot on a macroscopic level tell whether they are hydrated or contain contaminants. It is, however, a good enough qualification for the overall judgment of how these salts behave in relation to each other, particularly as none of these salts show identical/similar properties

or performances to one another. This is not only concerning for establishing trust and comparability across scientific papers, but also particularly concerning for anyone working on NGBs, where differences like these might result in a material falling out of favour. The resulting electrochemical performance of the salts A-E, on symmetric Ca||Ca cells in liquid and molten salt electrolytes has been explored further in section **5.4**.

The solubilities predicted in **Paper V** qualitatively, and sometimes even semi-quantitatively, somewhat match the experimentally observed data, but overall vary quite a lot from the experimentally extracted solubilities, especially relevant here for the Ca-salts. Even the experimental data taken from the literature vary from the experimental solubilities in this study. Any hydration issues arising from insufficient drying of salts and solvents cannot be cross-checked in the literature, but would cause solubility to increase dramatically. If also considering the differences seen from salt A-E from **Paper IV**, these would result in very different ΔG_{fus} as needed for COSMO-RS, also resulting in significantly different solubilities. When such fundamental properties as solubility, and melting and decomposition temperatures exhibit unreliability, it highlights the consequences that can result further along, both experimentally and computationally.

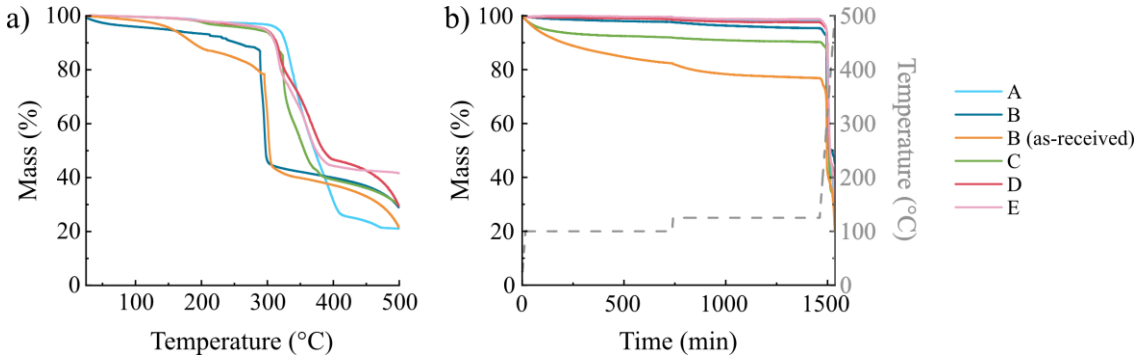

Figure 5.2 TGA traces of $Ca(FSI)_2$ salts A–E, where a) dynamic and b) isothermal.

The most extensive use of melting and decomposition temperatures in this thesis has still been to make an initial judgment of suitable MSEs, where all presented here is of equimolar compositions. From the vast opportunities of complexity MSEs present, from multi-anionic, multi-cationic, and mixed systems, as well as mixing salts of either the same or different charges (alkali *vs.* alkaline earth metals), the initial idea was to keep it rather simple. Thus, creating a multi-anionic MSE of only Ca-salts, $Ca[FSI\text{-}TFSI\text{-}NFSI]_2$, containing the salts $Ca(FSI)_2$, $Ca(TFSI)_2$, and $Ca(NFSI)_2$.

The benefit of keeping to just Ca^{2+} – that any metal plating and stripping with this type of MSE undeniably would be that of Ca – must be balanced with the drawback of these salts, which, while low for Ca-salts overall, are still rather high melting (**Figure 5.1b**). The heating trace of $Ca[FSI\text{-}TFSI\text{-}NFSI]_2$ shows small instabilities at various temperatures, which are hard to distinguish as peaks and consequently challenging to designate as a T_m (**Figure 5.3a**). Both single Ca-salts and multi-anionic MSEs, in general exhibit in more endothermic enthalpy of mixing, when compared to analogous alkali metal salts and with increasing size difference between the anions, respectively. This indicates that the fact that $Ca[FSI\text{-}TFSI\text{-}NFSI]_2$ shows no obvious melting peak does not necessarily mean it does not melt. The pragmatic approach was to place a vial containing the mixed MSE powder on a hot plate and gradually increase the temperature; even at 200 °C, after several hours, it

showed no sign of melting. The thermal decomposition was also evaluated, showing that the MSE has a lower T_d than the corresponding single salts (**Figure 5.3b**). It is expected that the weakest ion-ion interaction among the salts included in the MSE will also be the limiting factor in the MSE's stability. Both the lowered T_d and the lack of T_m indicate that Ca[FSI-TFSI-NFSI]$_2$ is not a good contender for further battery application tests.

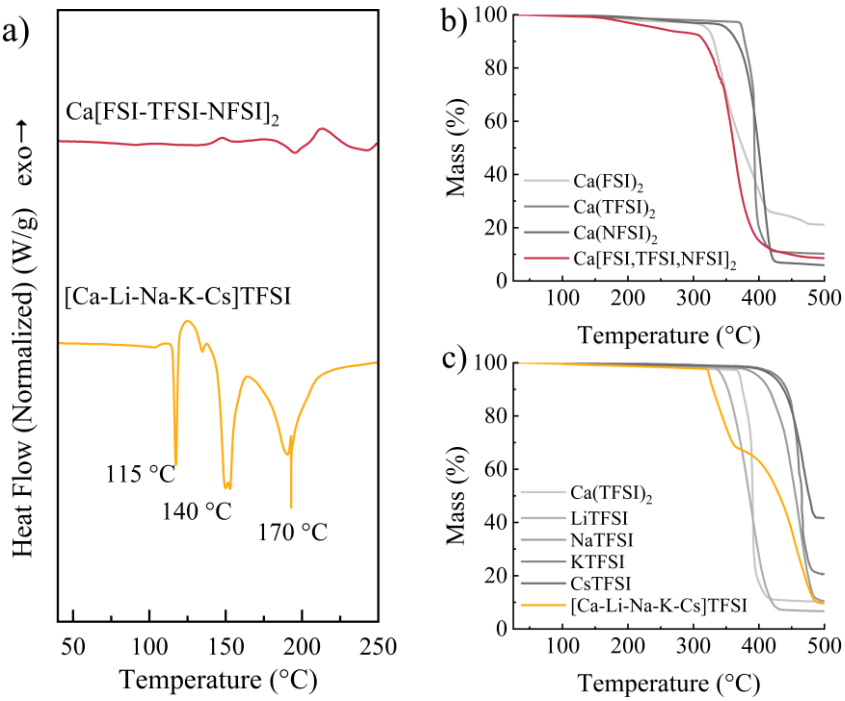

Figure 5.3 a) DSC heating traces and corresponding event temperatures of Ca[FSI-TFSI-NFSI]$_2$ and [Ca-Li-Na-K-Cs]TFSI. Dynamic TGA traces of MSEs and corresponding single salts of b) Ca[FSI-TFSI-NFSI]$_2$ and c) [Ca-Li-Na-K-Cs]TFSI.

The natural next step was to combine Ca^{2+} with monovalent cations. Going from cations of the same charge to those of different charges increases the complexity of the MSE, and, at least initially, to avoid further complexity, analogous TFSI salts of Ca, Li, Na, K, and Cs were used to create the multi-cationic quintenary MSE [Ca-Li-Na-K-Cs]TFSI. A quintenary MSE provides the opportunity of removing one or two alkali metal cations at a time, creating quaternary and ternary MSEs, and thus distinguishing the individual contributions of each cation.

A quintenary MSE also offers the potential for a much lower T_m than the corresponding single salts it contains; a necessity if intermediate (~60-80 °C) to high (80-120 °C) battery operation temperatures[7] are to be targeted. The heating trace of [Ca-Li-Na-K-Cs]TFSI, however, shows several melting peaks (**Figure 5.3a**), which could indicate that the equimolar composition is too far off from the eutectic. A bigger aspect is that when large cations like Cs^+ are combined with multivalent cations, there is an increased risk of forming complex AGGs, which will not yield an ideal, homogeneous melt. The dynamic TGA of [Ca-Li-Na-K-Cs]TFSI (**Figure 5.3c**) also shows two concerning features: (i) just like the case of Ca[FSI-TFSI-NFSI]$_2$, the MSE shows a lower decomposition temperature than the corresponding single salts, and (ii) the decomposition occurs in a stepwise fashion, a further

indication of non-ideal mixing. Cs^+ has shown impressive performance in alkali metal MSEs, but it does not, at least not paired with the TFSI-anion, seem to be the way forward for Ca^{2+}-containing ones.

Removing CsTFSI and creating the quaternary [Ca-Li-Na-K]TFSI together with corresponding ternary MSEs might yield more homogenous mixtures, but removing one or two salts will most certainly result in higher T_m, than that of the lowest of the melting peaks for the quintenary MSE. That peak appeared at 115 °C (**Figure 5.3a**) – a temperature already challenging for laboratory equipment and still requiring an additional >20 °C to provide sufficient internal dynamics for the MSEs to electrochemically cycle. Instead, the lower-melting alternatives, FSI-salts, were explored further, with the quaternary [Ca-Li-Na-K]FSI and corresponding ternary MSEs, in **Paper I**. Compared to TFSI, FSI has shown to have a stronger "caging" effect on the cations, which could potentially reduce their mobility;[112] however, lower mobility does not necessarily correlate with lower conductivity.[53]

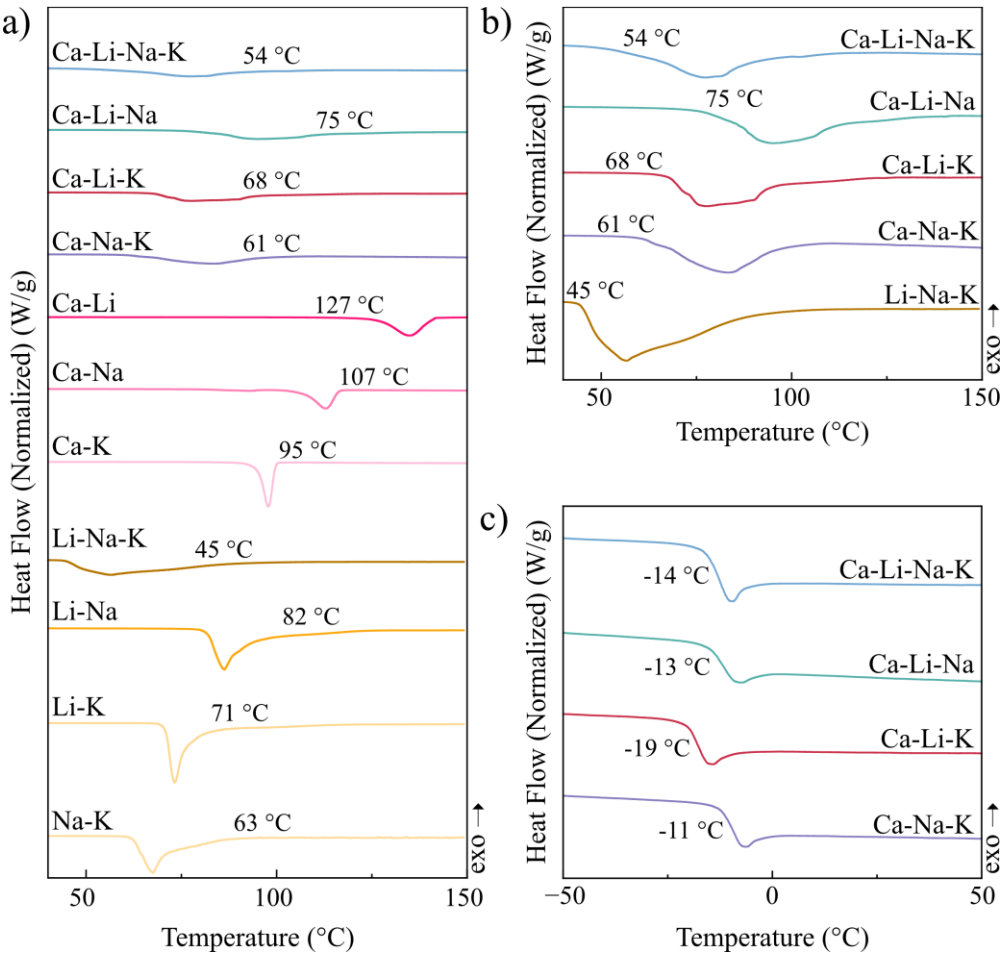

Figure 5.4 DSC heating traces and corresponding event temperatures of a) FSI-based MSEs, b) close-up of quaternary and ternary FSI-based MSEs, and c) glass transition of quaternary and ternary $Ca(FSI)_2$-based MSEs.

The T_m of the ternary and quaternary FSI-based MSEs lies between 54-75 °C (**Figure 5.4ab**), all as a single melting peak, indicating homogeneous mixtures. The T_m of these MSEs coincides with the literature T_m values for MSEs without Ca^{2+}, which raises the

question of whether Ca^{2+} is truly part of the MSEs. Tests of equimolar MSEs without Ca^{2+} show both slightly higher T_m but also steeper melting peaks than their Ca^{2+}-containing counterparts (yellow traces in **Figure 5.4a**), indicating that Ca^{2+} is indeed part of the created MSEs. After cooling and reheating the MSEs, they all exhibit a glass transition (**Figure 5.4c**), indicating inherent slow dynamics and non-equilibrium, the effect of which is shown in **Paper II**. For their decomposition, they all have similar T_d (**Figure 5.5**), which is intermediate to that of the included single salts in the MSEs.

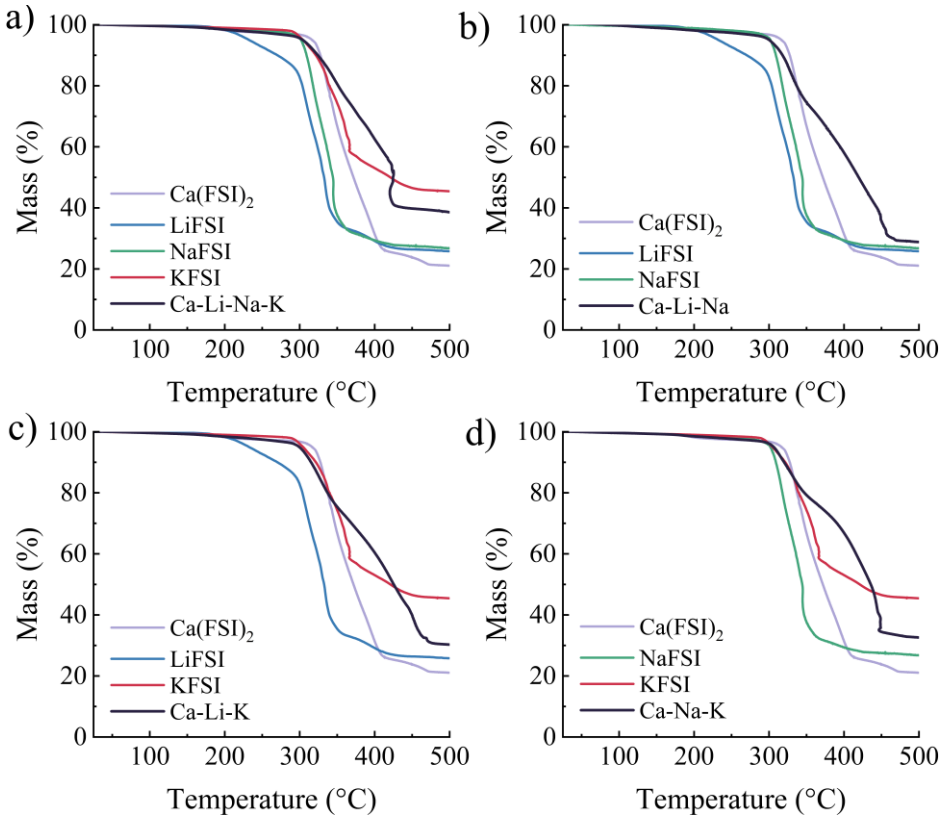

Figure 5.5 Dynamic TGA traces of MSEs and corresponding single salts of a) [Ca-Li-Na-K]FSI, b) [Ca-Li-Na]FSI, c) [Ca-Li-K]FSI, and d) [Ca-Na-K]FSI.

As all these MSEs on a first level of approximation create homogenous mixtures, the entropic effect and the role of each cation were studied further in **Paper I**. By adding binary $Ca(FSI)_2$-containing MSEs (pink traces in **Figure 5.4a**), the full range of possible combinations of quaternary, ternary, and binary MSEs provided by these four salts, reveals the relationship between T_m and ΔS_{mix} (**Figure 5.6**). While the lowered T_m for the quaternary MSE, in relation to the ternary Ca^{2+}-containing ones, is a result of higher entropy, *e.g.*, increased ΔS_{mix}, the ternary [Li-Na-K]FSI, which lacks Ca^{2+}, has the lowest T_m. This shows the challenges of creating truly low-melting MSEs that contain Ca-salt. Looking only at the difference between MSEs containing Ca^{2+}, it shows that the roles of differently sized cations and the tentative disorder created by these size differences can also be inferred; the MSE with the smallest ion radii differences, [Ca-Li-Na]FSI, also has the highest T_m. The local structure of these MSEs was further studied in **Paper I** and expanded upon in **5.2**.

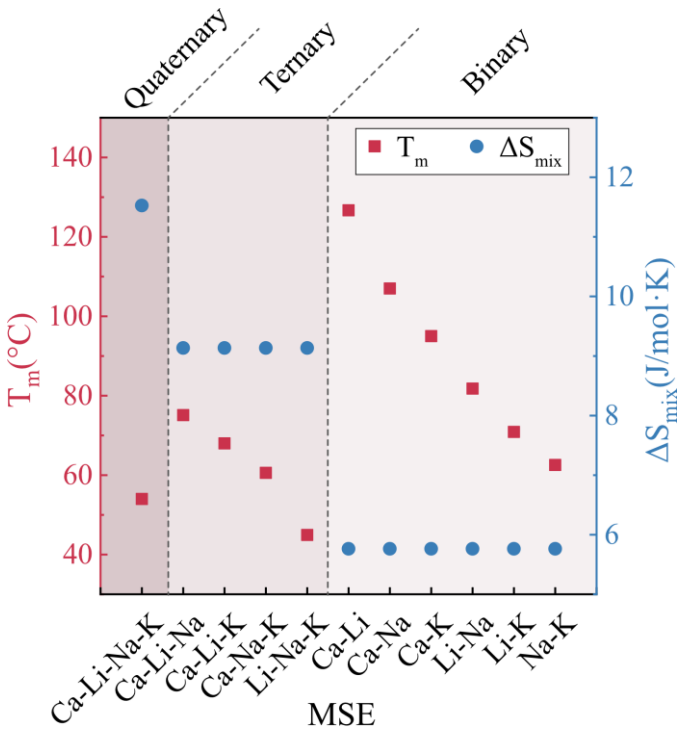

Figure 5.6 T_m and ΔS_{mix}, for the left-to-right, quaternary, ternary, and binary FSI-based MSEs.

The cycling of these MSEs in symmetric Ca||Ca cells is studied in **Paper II** and section **5.3**, where high-temperature CMBs have been targeted. Still, for potential future CMBs operating at intermediate temperatures (60-80 °C), even more complex high entropy MSEs were developed. With the very low melting analogous Li-, K- and CsFTFSI-salts as a base and combined with either $Ca(FSI)_2$, $Ca(TFSI)_2$, and $Ca(NFSI)_2$, referred to as CaA_2x[Li-K-Cs]FTFSI (A = FSI, TFSI or FTFSI), these mix both different cations and partially different anions. Both the heating traces of the MSE with $Ca(FSI)_2$ and with $Ca(TFSI)_2$ (**Figure 5.7a**) exhibit characteristic broad melting peaks, indicating a homogeneous melt, with particularly notable low T_m. This, despite containing Cs^+, which showed signs of inhomogeneous melting in the previously mentioned quintenary TFSI-based MSE. The $Ca(NFSI)_2$x[Li-K-Cs]FTFSI MSE, on the other hand, while having a sharp, deep melting peak, does not depress the T_m to the same extent. The $Ca(NFSI)_2$ salt, which was also part of the multi-anionic MSE $Ca[FSI\text{-}TFSI\text{-}NFSI]_2$ and was unable to melt below 200 °C, seems to be derogatory to these MSEs. The T_d of the MSEs in this group (**Figure 5.7b-d**) either corresponds to the lowest ion-ion interaction of the single salt or intermediate to the included single salts.

The mixtures of $Ca(FSI)_2$ or $Ca(TFSI)_2$ in [Li-K-Cs]FTFSI show indications of favorable MSEs and should perhaps be tested further. Together with the multi-anionic and multi-cationic MSEs shown here, they complete the picture of varying complexities available to create higher entropy and thus, lower melting points. The difficulties and the promises of creating Ca^{2+}-containing MSEs – together with input for computational models and estimates of differences in salt formulations from different suppliers – show the broad utility thermal properties provide.

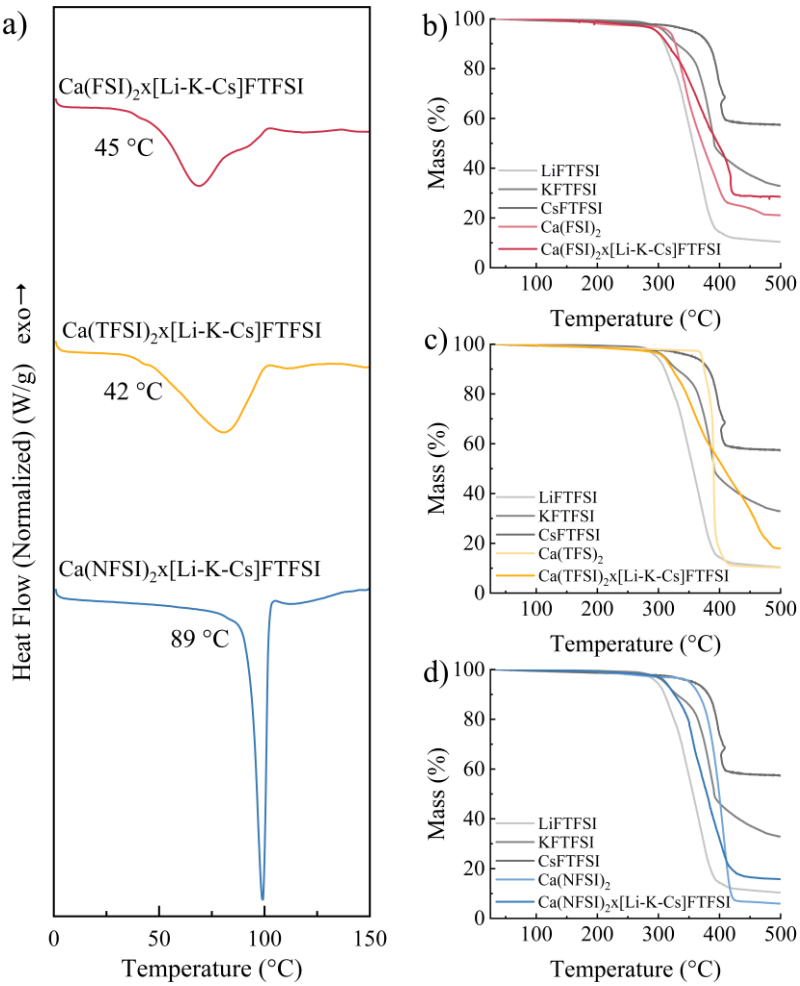

Figure 5.7 a) DSC heating traces and corresponding event temperatures of $Ca(FSI)_2$x[Li-K-Cs]FTFSI, $Ca(TFSI)_2$x[Li-K-Cs]FTFSI, and $Ca(NFSI)_2$x[Li-K-Cs]FTFSI. Dynamic TGA traces of MSEs and corresponding single salts of b) $Ca(FSI)_2$x[Li-K-Cs]FTFSI, c) $Ca(TFSI)_2$x[Li-K-Cs]FTFSI, and d) $Ca(NFSI)_2$x[Li-K-Cs]FTFSI.

5.2 Local structure of electrolytes

The local structure of MSEs and liquid electrolytes, as seen *e.g.* by Raman spectroscopy, provides different levels of complexity: for MSEs, which are solvent-free, "only" ion-ion interactions need to be considered, albeit they can be very complicated, whereas the analysis of liquid electrolytes must balance ion-ion and ion-solvent interactions. For the ternary and quaternary MSEs in **Paper I**, the region of main interest is the spectral range 650-850 cm^{-1} (**Figure 5.8a**), containing the FSI anion's "all breathing mode".[113] The "free" FSI anion, in solution/electrolytes is reported at 720 cm^{-1},[114,115] which in the different salts overall shifts to higher wavenumbers, with a size of the shift according to the polarizing power of the cation. The exception is $Ca(FSI)_2$, as despite Ca^{2+} having a larger polarizing power than Li^+ does,[63] shifts marginally less: the band is positioned 772 cm^{-1} for $Ca(FSI)_2$ *vs.* 773 cm^{-1} for LiFSI. KFSI has a different crystal structure compared to the other salts,[116] which could potentially explain why the band in this region splits.

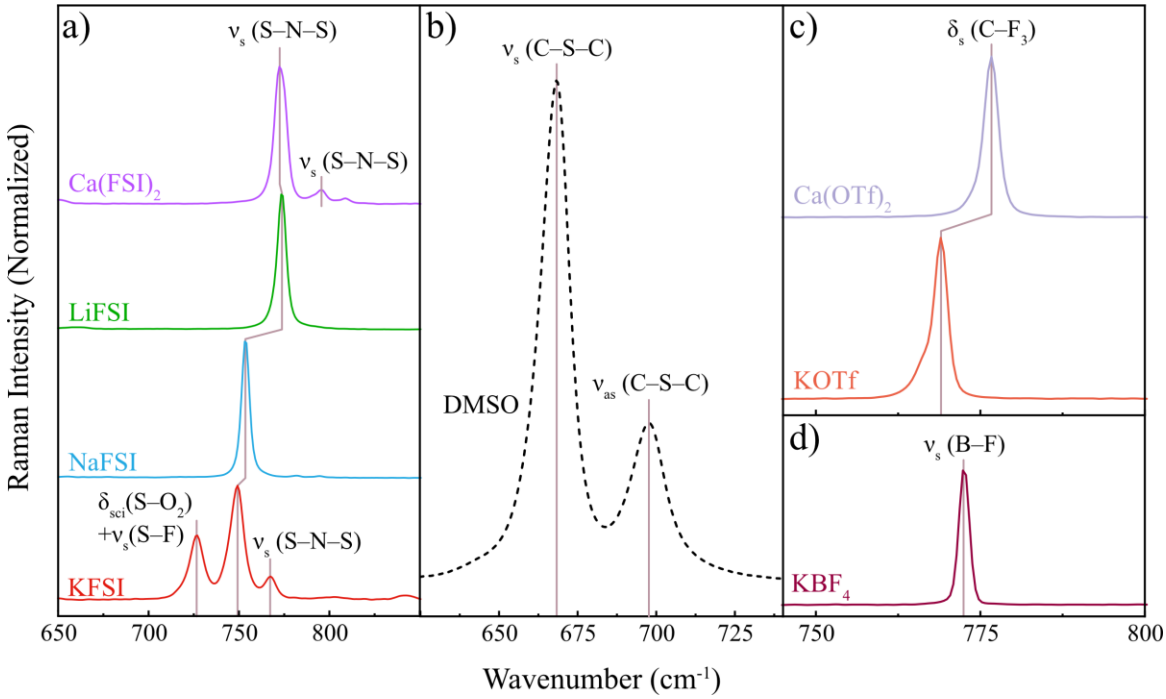

Figure 5.8 Raman spectra of a) single FSI-salts, b) DMSO, c) single OTf-salts, and d) single KBF_4-salt.

For the liquid electrolytes in **Paper III**, which combine analogous Ca- and K-salts of OTf and BF_4 in DMSO, there are three regions of interest, in which bands from the solvent and neither of the anions overlap. In DMSO, the most prominent bands are the symmetric and asymmetric stretching of the S–N–S bonds seen at 668 and 698 cm^{-1} (**Figure 5.8b**), respectively.[117] For OTf^-, the chosen band, symmetric stretching of the C–F_3 bond, appears as a "free" anion at 766 cm^{-1},[118] which, just like the FSI-salts, shifts to a higher wavenumber (769 cm^{-1} for K^+ *vs.* 777 cm^{-1} for Ca^{2+}), according to the cation polarizing power (**Figure 5.8c**). BF_4^- as a "free" anion appears at 760 cm^{-1},[119] shifting to a higher wavenumber for KBF_4 (772 cm^{-1}) (**Figure 5.8d**).

The spectra of pure KBF_4 salt overlap with those of the OTf-salts, but when dissolved in DMSO, they do not (**Figure 5.9**). Instead, the bands of the OTf-based electrolytes shift to 752 cm^{-1} and the BF4-based to 763 cm^{-1}, where neither shows any detectable shift when comparing Ca^{2+} *vs.* K^+. Ca-salt electrolytes, which due to the Ca^{2+} cation's divalent nature have a higher anion concentration, show greater intensity than K-salt electrolytes. In all cases, as the salt concentration increases, the band intensities also increase, as expected. Deconvolution reveals that K-salt electrolytes have a higher percentage of CIPs than their Ca-salt counterparts, with BF_4-based having more than OTf-based.

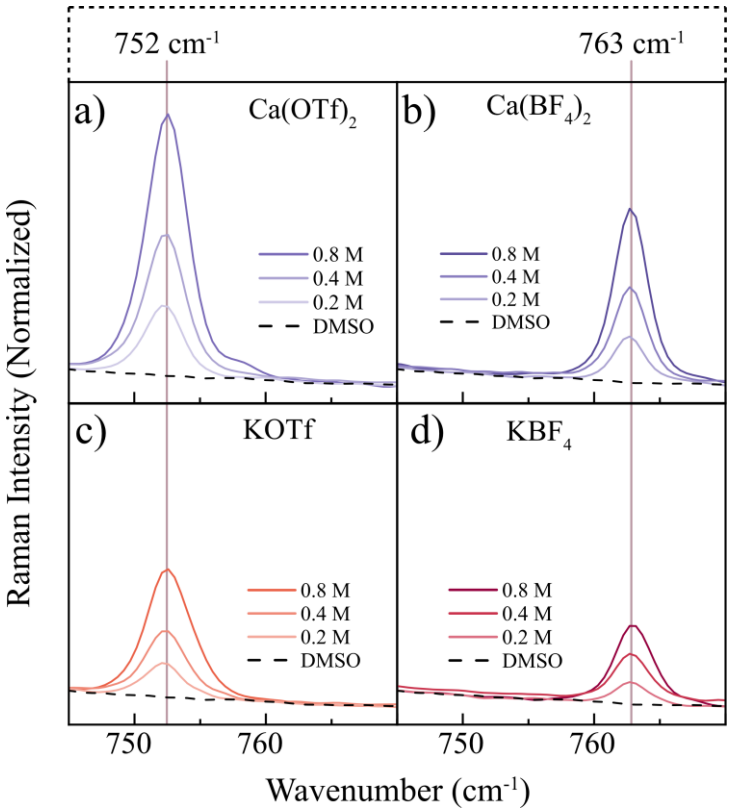

Figure 5.9 Raman spectra of the concentration dependence for ion-ion interactions of single salts in DMSO, where a) $Ca(OTf)_2$, b) $Ca(BF_4)_2$, c) KOTf, and d) KBF_4.

Looking at the ion-solvent interactions, the Ca-salt electrolytes (**Figure 5.10ab**) show decreasing intensity of the unperturbed DMSO bands and the appearance of cation-induced shoulders at ~678 and ~712 cm^{-1}, as a function of salt concentration. The K-salt electrolytes (**Figure 5.10cd**), on the other hand, show spectra much closer to that of pure DMSO regardless of concentration. As the polarizing power of K^+ is not as strong as that of Ca^{2+}, it is indeed expected that the K-salt electrolytes will have more "free" DMSO. This agrees with observations of ion-ion interactions: weaker ion-solvent interactions naturally mean that fewer ions bind to solvent molecules and instead bind to other ions, *e.g.,* renders more CIPs in the K-salt electrolytes.

With no solvent present, as in the FSI-based MSEs, all of which are equimolar, the concentrations have not been varied; instead, correlations are drawn according to salt composition. Typically, for the multi-cationic MSEs, the Raman spectra are expected to be simply additive, with the fraction of each salt corresponding to the overall features of the spectrum.[120] Mixing in the divalent Ca^{2+} ion via Ca-salt with alkali metal salts, however, introduces different charges; thus, the spectra cannot be guaranteed to be additive. In **Figure 5.11a**, all Ca-based MSEs show a strong, broad band centered at *ca.* 771 cm^{-1} with a shoulder, both of which are signatures of disordered and local structures out of equilibrium. Also present is a less intense band at *ca.* 795 cm^{-1}, indicating the influence of Ca^{2+}. A reference containing no $Ca(FSI)_2$, Li-Na-K, was added, which only has one single broad band at 761 cm^{-1}. Thus, Li-Na-K has the more expected additive appearance of multi-cationic mixtures with the same charges – highlighting Ca^{2+} influence on the local structure of the other MSEs.

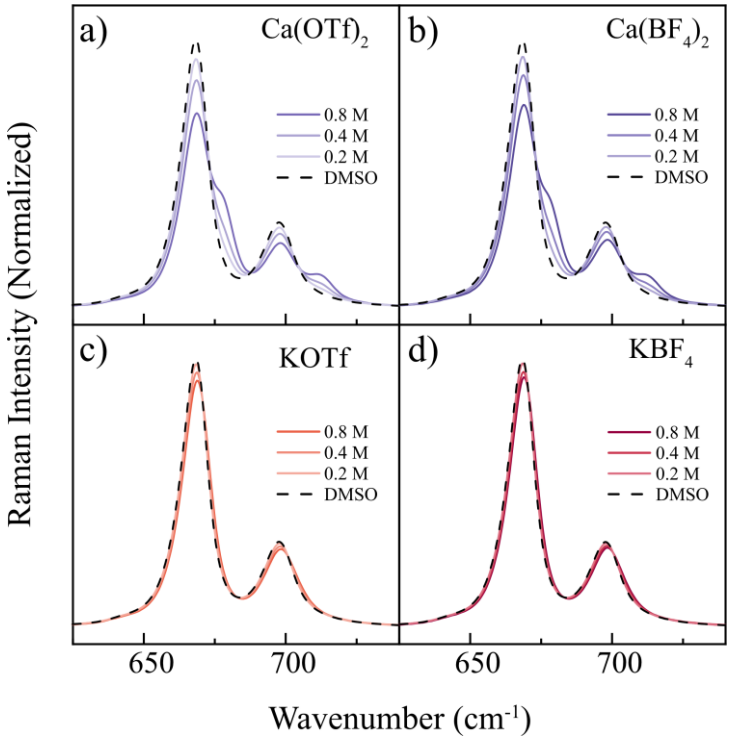

Figure 5.10 Raman spectra of the concentration dependence for ion-solvent interactions of single salts in DMSO, where a) $Ca(OTf)_2$, b) $Ca(BF_4)_2$, c) KOTf, and d) KBF_4.

Considering the compositional effects and the possible entropic stabilization of the local structure, one of our design hypotheses, the MSEs were studied not only in their "as cast" state but also after natural aging (**Figure 5.11b**). While the structure of the quaternary MSE, Ca-Li-Na-K, remains the same after one week of ageing, the ternary MSEs all see a change in the spectra, and in the case of the MSEs containing KFSI, the appearance of two new bands at 727 and 749 cm^{-1}, corresponding partially to (re-)crystallized/micro-separated KFSI. The difference observed in the Li-Na-K reference, combined with the fact that the quaternary MSE shows a significant change in local structure only after further aging (>2 weeks), indicates that the stabilizing effect can be partially attributable to its higher entropy.

The MSEs and liquid electrolytes presented here both exhibit pronounced spectral changes due to the strong Coulombic interactions of the Ca^{2+} cation. While liquid electrolytes are harder to deconvolute and to draw accurate representations of ionic species, varying the cationic and anionic species and their concentrations sheds light on how these species interact relative to each other. Similarly, by comparing the time dependence of Ca-based MSEs with that of the reference, it is possible to distinguish the effects of Ca-salt *vs*. entropic effects in these types of electrolytes.

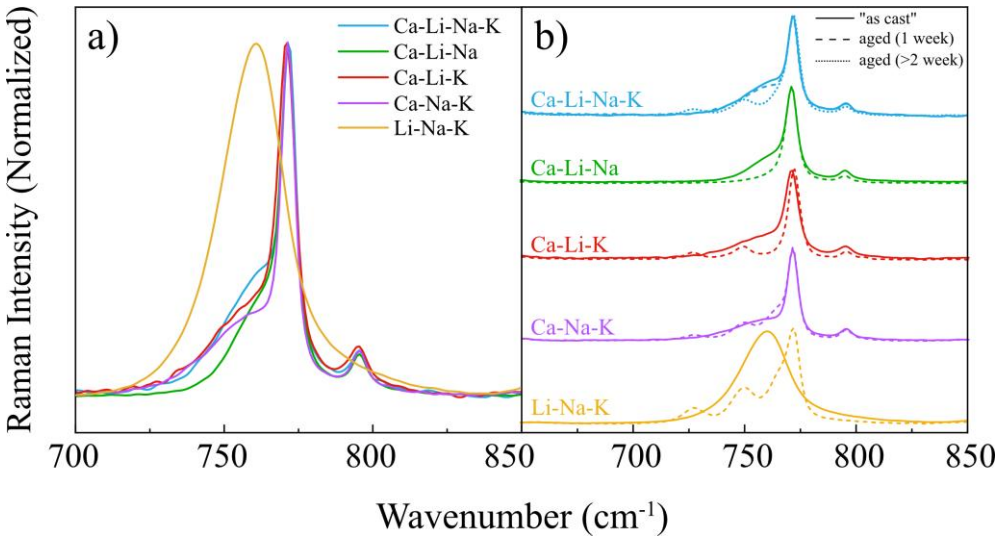

Figure 5.11 Raman spectra of MSEs: a) combined "as cast", and b) both "as cast" and aged.

5.3 Plating and stripping on Ca metal anodes

Ca metal plating and stripping, severely challenged by the lack of standard cathodes for electrolyte testing, has so far been enabled by liquid electrolytes. As such, the MSEs presented here really are the initial first steps and are only in a proof-of-concept stage. By comparing the Ca-, K-, and mixed-salt electrolytes in **Paper III** with the MSEs presented in **Paper II**, an attempt is here made to present where MSEs presently stand, and where they would need to go to enable long-term cycling. In **Paper III**, the most performant electrolytes were those based solely on KBF_4 or KOTf, in terms of the lowest potential and the longest cycling time, respectively (**Figure 5.12a**). Compared to analogous Ca-salt electrolytes, the improvement seen was up to 300 hours of cycling.

The most performant MSE of **Paper II**, Ca-Na-K, which compared with the other MSEs had the lowest charge density of the additional cations, had in contrast, much higher potential (>2 V) and shorter cycle length (<15 h) (**Figure 5.12b**). The voltage saw a lowering with a pre-program (applied current density of 0.05 mA/cm² until -3.5 V was reached, after which regular galvanostatically cycling at 0.02 mA/cm² started), but only upon oxidation (**Figure 5.12c**). Applying the same pre-program to two identical cells, then disassembling them and pairing the oxidized (reduced) electrodes within new cells, showed that the pre-oxidized cells failed rapidly (**Figure 5.12d**). The pre-reduced cell instead showed a large improvement with low voltage maintained both upon oxidation and reduction, but only for 5 cycles, after which it rapidly increased in voltage (**Figure 5.12e**).

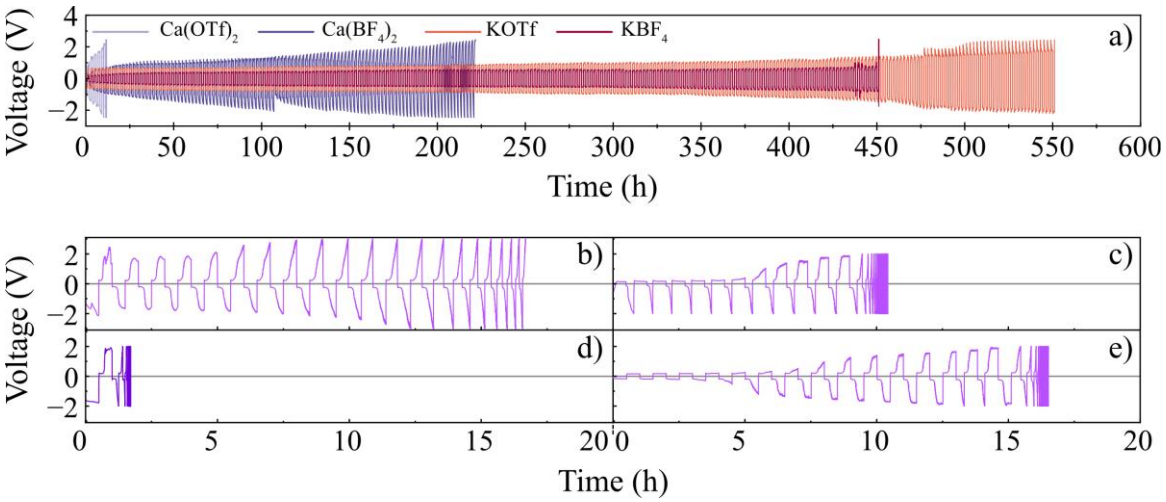

Figure 5.12 Galvanostatic cycling of symmetric Ca||Ca cells: a) 0.8 M liquid single Ca- and K-salt electrolytes at 0.02 mA/cm², and a Ca-Na-K MSE cycled with: b) no pre-program (0.02 mA/cm²), c) with pre-program, d) pre-oxidized electrodes, and e) pre-reduced electrodes (0.05 mA/cm² until -3.5 V, then 0.02 mA/cm²).

An overview of all the electrolytes explored in **Paper II** and **III**, in terms of average cycling voltage after 50 h (adjusted to voltage at first oxidation for MSEs) and the cumulative cycling time is shown in **Figure 5.13a**. Starting from the liquid electrolytes, the Ca-salt based, both as single electrolytes at different concentrations and dual at a fixed 0.8 M salt concentration, are by far the least performant. Those of dual-salt at fixed concentration saw much improvement over the Ca-salt electrolytes and overtook the KOTf-based at lower concentrations but did not exceed the single K-salt 0.8 M electrolytes. The MSEs, on the other hand, appear in the very far left, showing how far they yet must come in terms of cycle length. Looking at the voltage at the first cycle of the MSEs (**Figure 5.13b**), paints a far more promising picture, as all have a voltage of ≤0.15 V – exceptionally low for Ca electrolytes.

Overlaying the initial cycling (0.02 mA/cm²) of the most performant MSE – the pre-reduced cell of Ca-Na-K – with the single liquid electrolytes based on $Ca(BF_4)_2$, KOTf, and KBF_4 at 0.8 M (**Figure 5.13c**), shows that Ca-Na-K has a lower voltage than those of $Ca(BF_4)_2$ and KOTf (~0.5 V), and performs just as well as the KBF_4-based. The two main challenges for Ca metal anodes and Ca battery electrolytes are the sluggish movement of the Ca^{2+} ions and the passivation of the Ca metal interface. The low voltage of the Ca-Na-K MSE indicates that the ions have enough internal dynamic movement to facilitate cycling, but the short number of cycles – 5 cycles (Ca-Na-K) *vs.* >200 cycles (KBF_4-based) – indicates that the decomposition products of the MSE most likely passivate the surface rather than enhancing it.

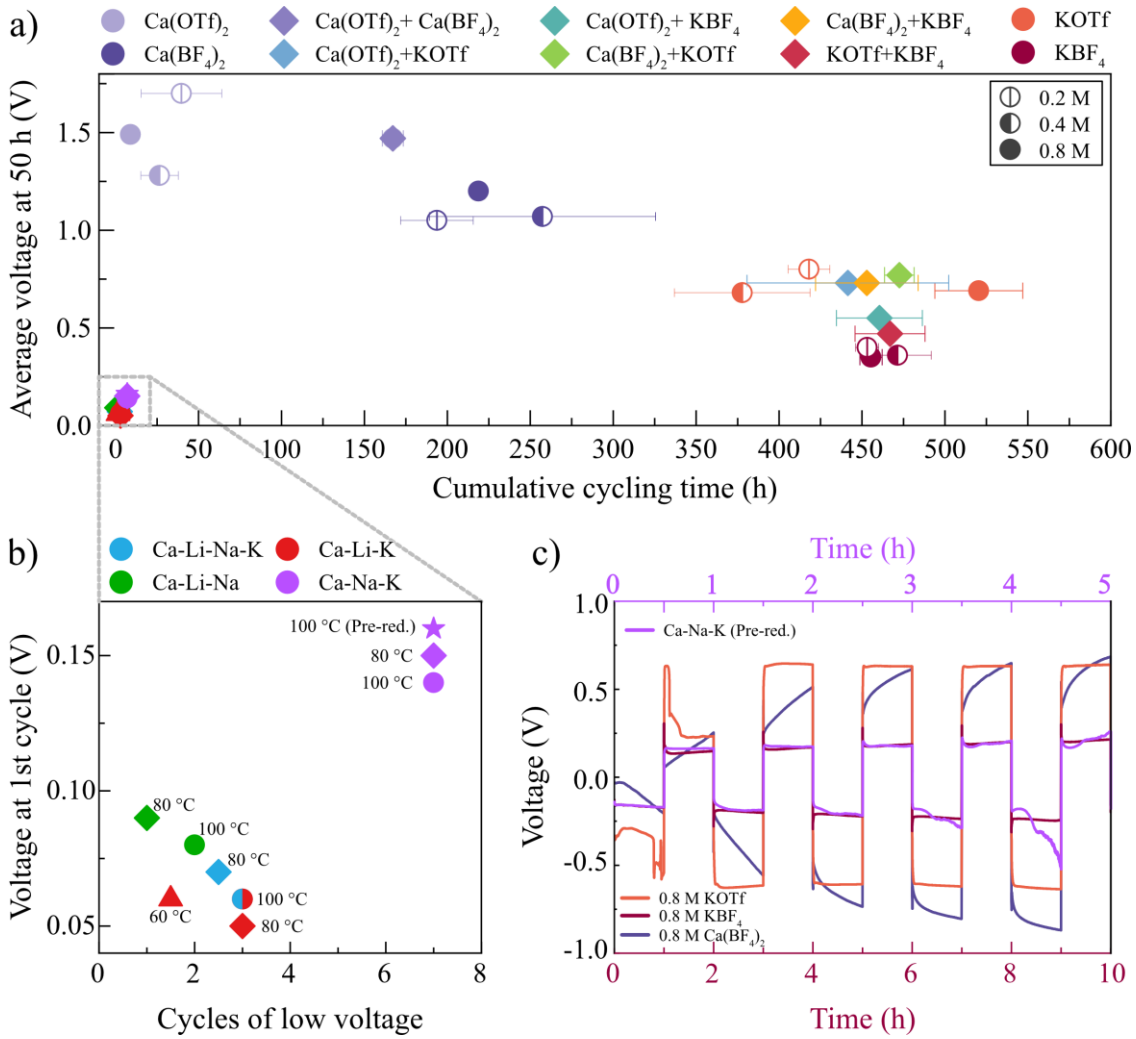

Figure 5.13 Galvanostatic cycling of symmetric Ca||Ca cells, showing a) average voltage at 50 h vs. cycling time, b) voltage at 1st cycle vs. cycles of low voltage at oxidation for MSEs, and c) initial cycling of selected liquid electrolytes and pre-reduced cell of Ca-Na-K MSE.

Symmetric cells offer an indication of electrolyte performance, but do not provide full insight into true reversible plating and stripping. The CV of the quaternary Ca-Li-Na-K MSE and the 0.8 M single K-salt electrolytes (**Figure 5.14**) has been conducted under significantly different conditions: the MSE at 100 °C with a scan rate of 25 mV/s in a three-electrode beaker cell, using Au as the WE and Ca as both the CE and RE; and the liquid electrolytes at room temperature with a scan rate of 20 mV/s in a two-electrode coin cells, with stainless steel (SS) as WE and Ca as CE/RE. Nonetheless, this comparison offers an interesting point of insight. In the Ca-Li-Na-K MSE (**Figure 5.14a**), a prominent redox process is observed, with a notably high anodic stability. Upon positive sweep, two peaks can be seen in the voltammogram, indicating that multiple metal redox reactions may occur. Although only cycled for 4 cycles, no passivation is observed.

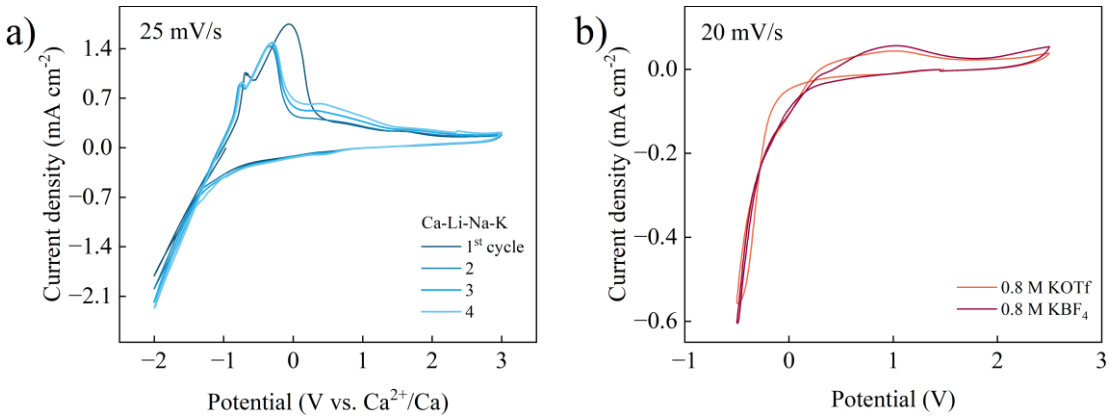

Figure 5.14 Cyclic voltammograms of: a) three-electrode (Ca||Ca||Au) cell of Ca-Li-Na-K at 100 °C, and b) two-electrode coin cell (Ca||SS) at room temperature.

Both the liquid K-salt electrolytes have observable redox processes (**Figure 5.14b**), though to a much lesser extent than the MSE. Only the 1st cycle is shown, as both electrolytes gradually passivate the SS surface. Au is a more suitable WE for Ca electrolytes than SS, though it is less so for alkali salt electrolytes, as alloying may occur. For morphological and compositional analysis, the liquid K-salt electrolytes were electrochemically reduced in a Ca||SS half-cell configuration, and SEM and EDX imaging of the extracted SS electrode was conducted (**Figure 5.15**). The deposits formed by the KBF_4-based electrolyte show two types of structures: small granules containing K and F, and larger flower-like structures containing K, C, O, and very little Ca. This is consistent with prior reports on using an electrolyte of KPF_6 in EC:DMC:EMC, which also showed plating of both Ca and K on a gold electrode.[65] The KOTf-based electrolyte, on the other hand, have an evenly spread, interconnected petal-like morphology, which, with EDX-mapping, shows to be mostly Ca, together with O, C, and F.

While liquid electrolytes by far outperform MSEs in symmetric cells in terms of life length, the low voltage of MSEs, as well as the prominent redox processes observed by CV, gives hope for future MSE development. Neither of the electrolyte concepts has yet been tried in full cells, and while this brings its own set of challenges, no electrolyte should be completely discounted until it has been tried.

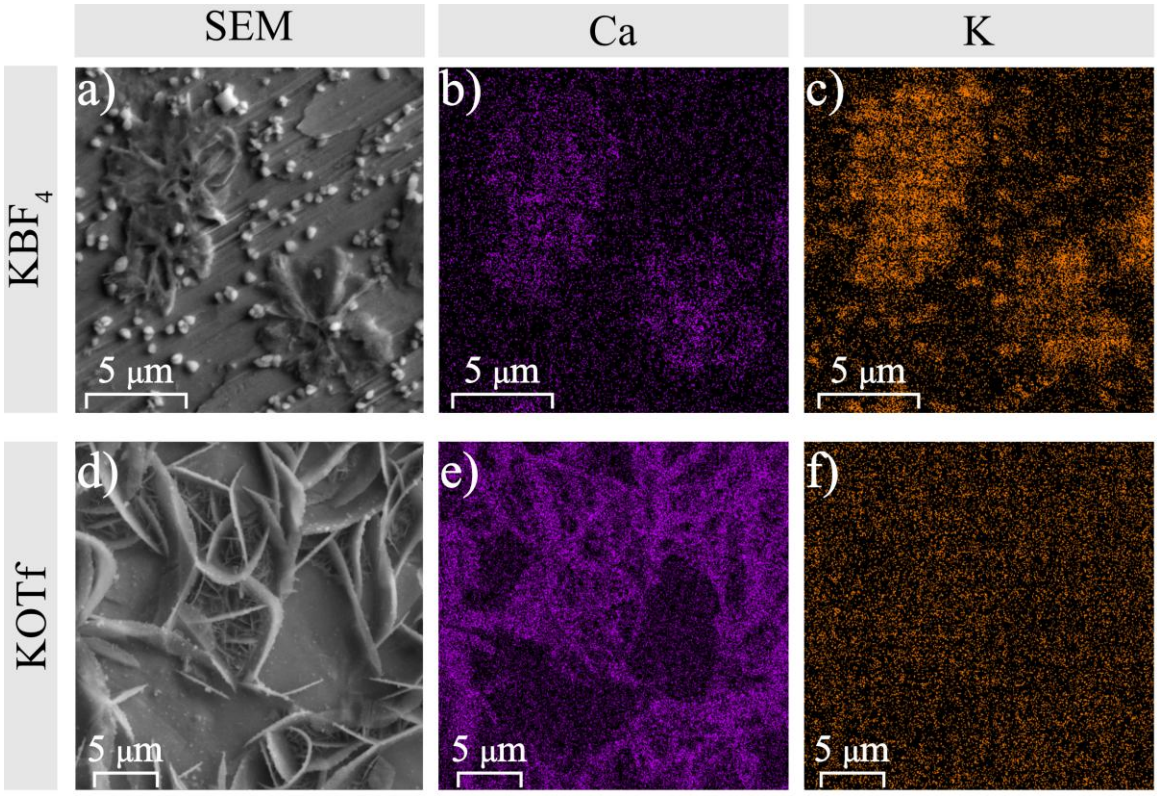

Figure 5.15 SEM and EDX mapping of deposition on a SS electrode, using liquid K-salt electrolytes, where a-c) KBF_4-based, and d-f) KOTf-based.

5.4 Impact of salt purity on cyclability

Electrolyte salts are a class of materials that have historically experienced contamination issues caused during synthesis. Researchers put their trust in commercially sourced materials and as such should expect comparability across scientific studies. When $Ca(FSI)_2$ salt from five different suppliers A-E was assessed in **Paper IV**, as well commented upon in section **5.1**, it was shown that there were quite a few differences between fundamental thermal properties. In particular, salt B showed a very different T_m to the other salts, and salt B again, but also salt C, saw large mass losses during dynamic and/or isothermal TGA. Following this, salts A-E have also been tested in different electrolyte formulations, both liquid electrolytes and MSEs, and in electrochemical tests, including full cells and symmetric cells.

In Ca||PTCDI full cells, electrolytes of salts A-E at 0.1 M concentration in DMAc (**Figure 5.16ab**), all electrolytes show reassuringly similar discharge capacities. Only salt B shows marginally worse discharge capacity as well as a higher voltage upon charging. Because readily available cathodes for CMBs are not available for testing subtle salt differences in long-term cycling behavior, symmetric Ca||Ca cells are employed (**Figure 5.16c**). Initially, all symmetric cells have a stable voltage of ±1.15 V, which persists until 250 h; thereafter, differences begin to appear. Ranking overall performance by lowest voltage and longest cycling time yields the following: B < C/D < E < A.

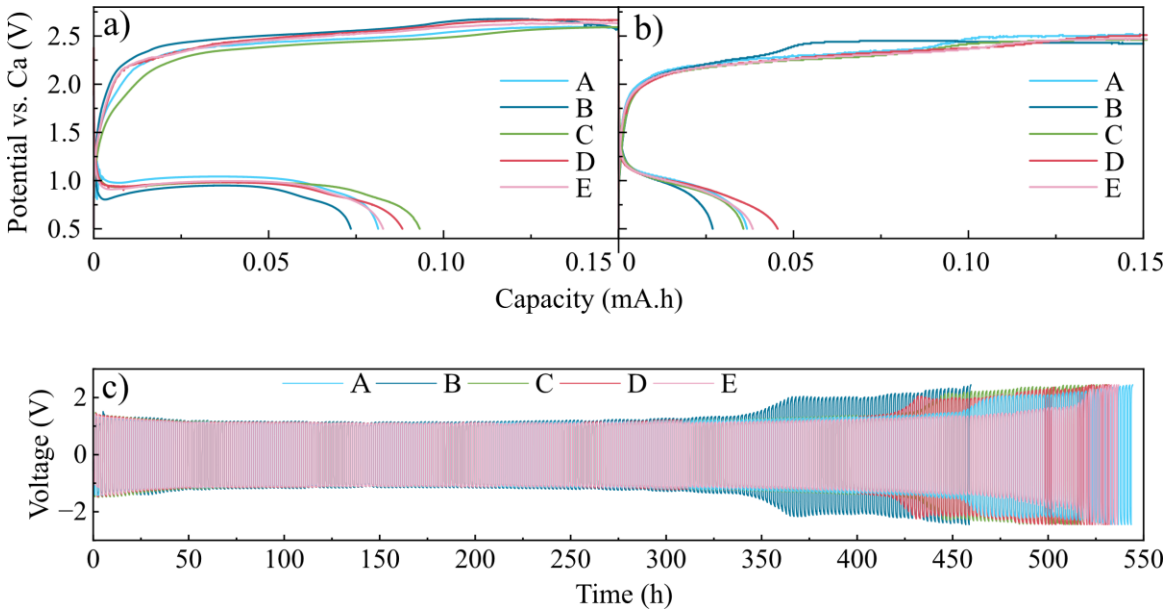

Figure 5.16 Galvanostatic cycling at room temperature of Ca(FSI)2 salts A-E in liquid electrolytes at 0.1 M concentration in DMAc, where a) and b) are voltage profiles of Ca||PTCDI full cells for the 2nd (a) and 7th (b) cycle, and c) long-term cycling in symmetric Ca||Ca cells.

The limitations of the PTCDI cathode, together with the low concentration in both cell configurations, might not capture the subtle differences in quality among these salts. Much more complex cell configurations containing MSEs, which are solvent-free and thus contain a high concentration of the $Ca(FSI)_2$ salt employed, do just that. Comparing the Ca-Na-K MSE, made by three of the different $Ca(FSI)_2$ salts – A, B (dried and as-received), and E, using the program presented in **Paper II** and section **5.3** (applied current density of 0.05 mA/cm² until -3.5 V is reached; thereafter, galvanostatically cycled at 0.02 mA/cm², with a cut-off voltage of ±2 V) – shows clear differences (**Figure 5.17**).

As previously, the cells exhibit low voltage hysteresis only upon oxidation. Salt A, used in **Papers I** and **II**, exhibits low-voltage hysteresis for 7 cycles. Salt B, in its as-received state, also has low voltage for 7 cycles, but the reaction occurs below 0 V. In its dried state, salt B behaves very differently: the oxidation voltage now occurs above 0 V, but only for 2 cycles; thereafter, very large voltage occurs on both oxidation and reduction. Salt E, which in **Paper IV** was seen as having the second-best overall performance after salt A, shows low voltage for 2 cycles, then a rapid increase in voltage, reaching the cut-off voltage far before any of the MSEs based on the other $Ca(FSI)_2$ salts.

MSEs, which should be fundamentally safer than liquid electrolytes for high-temperature battery applications, as two of their great benefits are: (i) no risk of solvent degradation nor ignition/flammability, and (ii) no vapor pressure build-up – now come into question. While the exact synthesis routes are secrets of the companies making the salts, the potential contaminants present cannot be excluded as non-organic, thereby increasing the flammability risk. Any decomposition products in the electrolyte, as seen, are detrimental to the already sensitive Ca metal anode.[10] Furthermore, the large mass loss observed in salt B indicates that the electrolyte lacks the high thermal stability it should have, and thus, gas evolution in the cell is likely. Maybe most concerning of all is that none

of these salts show identical or similar properties or performance, making these safety concerns a gamble.

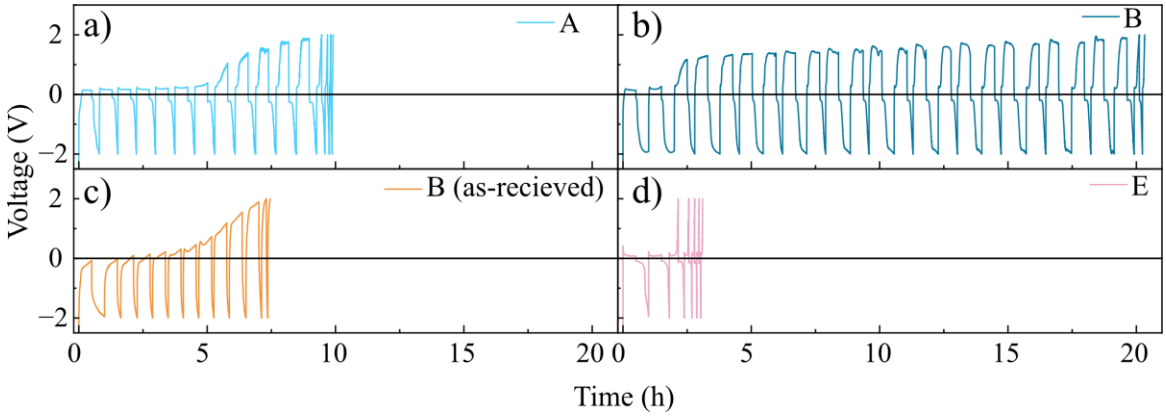

Figure 5.17 Galvanostatic cycling at 100 °C of Ca-Na-K MSEs in symmetric Ca||Ca cells, where the Ca(FSI)2 is from supplier a) A, b) B, c) B (as-received), and d) E.

Chapter 6

Conclusions and Outlook

Old salt: An experienced and weathered sailor, or someone with a lot of life experience

Navigating a ship safely across the ocean is not unlike the challenges faced in advancing NGB technologies. Passivation layers on Ca metal anodes are prevalent, and a healthy dose of skepticism is certainly needed for the long journey ahead. But behind creative electrolyte concepts, unconventional cell designs, and fine-tuning of the setup lies the promise of discovering *terra incognita*. The results presented in this thesis, has from the perspective of the electrolyte salts employed, attempted to provide potential solutions that can be translated into practical CMBs in the future. Something especially challenging when the nautical chart of Ca is shown to be quite different from that established for Li.

For hard work not to be of nought, commercial salts from different suppliers should yield the same physico-chemical properties. Running out of the $Ca(FSI)_2$ salt for **Paper II** from one supplier and being forced to switch to another meant that previous results could not be reproduced and that intended experiments were not completed. Though not everything is lost at sea. **Paper IV** was born, in a call for caution for anyone working within NGB R&D. Learnings from a decade more of LiFSI synthesis know-how, ideally, should be accordingly reflected. But just as the synthesis of $Ca(FSI)_2$ seems not as straightforward, the same could be said for the model presented in **Paper V**. Large deviations obtained *vs*. experimental data, particularly for Ca and Mg, showed that computational models take time to be adaptable for multivalent ions as well.

Behind the difficulties is the strong Coulombic interactions of the Ca^{2+} cation, which also have a pronounced effect on the local structure of MSEs and liquid electrolytes, as seen in **Papers I** and **III**. This is not to say that Ca^{2+} makes a bad situation worse, but rather that new ways of thinking need to be adopted. In **Paper III**, though, Ca^{2+} was seen to strongly interact with the solvents, K^+ did less so. K^+ instead interacted more strongly with other ions, forming more CIPs. Still, the KBF_4-based electrolyte enabled the lowest voltage, and the KOTf-based electrolyte enabled the longest cycle time. In both cases, but particularly the KOTf-based, deposition of Ca was possible, indicating that Ca^{2+} must have been part of the electrolyte at some stage, even if it was not initially so.

Liquid electrolytes for CMBs, while still under development, have had the time for several design strategies to emerge. The MSEs presented in **Papers I** and **II**, the first of their kind, are in contrast only at a very first proof-of-concept level. In **Paper I**, the structure of the Ca-based MSEs was shown not to be simply additive as compared to the non-Ca-based reference. Furthermore, the time-dependent stabilization of the local structure was also partially affected by the increased entropy of mixing as seen for the quaternary MSE.

Employing the same MSEs in **Paper II**, the increased entropy of the quaternary MSE did not make it the most performant. It was rather the charge density of the additional cations that had the most significant effect; the lowest cation charge density yielded the best cycling performance.

Combining the learnings of **Papers II** and **III** in section **5.3**, showed that the most performant MSE – the pre-reduced cell containing Ca-Na-K – initially had just as low voltage as the KBF_4-based liquid electrolyte, indicating that semi-solid MSEs for high-temperature CMBs can be a feasible route forward. From the literature it is known that in electrolytes containing only Ca-salt, the addition of boron matters substantially. But in the absence of Ca-salt, we find that when using K-salt with or without boron, the boron-containing electrolyte is not necessarily the one that performs the best. To confirm what species that are present in the interphase, the SEI would need to be studied directly, which could be an objective for future studies.

As the liquid K-salt electrolytes enabled Ca metal plating without the addition of Ca-salt, it suggests that *if* multi-cationic MSEs, Ca-based or not, can overcome passivation layers, they have the potential to do so as well. Exploring non-Ca-based MSEs for CMBs would enable simplified design requirements, as presented in the unpublished work section **5.1**; they would not be reliant on the high T_m of Ca single salts, and the difficulty of creating homogeneous mixtures from salts with different charges could be avoided. In the same section, MSEs of mixed cations and anions – $Ca(FSI)_2$ or $Ca(TFSI)_2$ in a base of [Li-K-Cs]FTFSI – showed promise for being particularly low melting. These MSEs never received the priority needed to come to fruition, but this shows that there still is more to explore for MSEs aimed at CMBs.

The electrolyte concepts in this thesis have only been tested in symmetric cells, but for reliable electrolyte testing, full cells are necessary. Still, as CMBs' development is in its infancy, cathodes are being researched in parallel. Few cathodes have been found, and those tested/compatible for high-temperature applications are scarce. Patience is therefore needed for CMBs to be deserving of the work employed, particularly at a time when commercialization has yet to be seen on the horizon. From the electrolyte concepts and cell designs brought forward here, some unconventional and more exotic – do know that we strive to bring batteries based on abundant raw materials to harbor. So that the development of CMBs is more than just the tales of an *old salt*.

Bibliography

(1) Aurbach, D.; Skaletsky, R.; Gofer, Y. The Electrochemical Behaviour of Calcium Electrodes in a Few Organic Electrolytes. *The Electrochemical Society Softbound Proceedings Series* **1991**, *138* (12), 3536–3545. https://doi.org/10.1149/1.2085455.

(2) Ponrouch, A.; Frontera, C.; Bardé, F.; Palacín, M. R. Towards a Calcium-Based Rechargeable Battery. *Nat. Mater.* **2016**, *15*, 169–172. https://doi.org/10.1038/nmat4462.

(3) *The Battery Report 2024 (Volta Foundation)*; Volta Foundation, 2025. https://report.volta.foundation/annual-battery-report/public/Battery_Report_2024.pdf.

(4) Haynes, W. M.; Lide, D. R.; Bruno, T. J. Abundance of Elements in the Earth's Crust and in the Sea. In *CRC Handbook of Chemistry and Physics*; CRC Press, 2017; pp 14–17.

(5) Brunklaus, G.; Lennartz, P.; Winter, M. Metal Electrodes for Next-Generation Rechargeable Batteries. *Nature Reviews Electrical Engineering* **2024**, *1*, 79–92. https://doi.org/10.1038/s44287-023-00006-5.

(6) Bitenc, J.; Ponrouch, A.; Dominko, R.; Johansson, P.; Palacin, M. R. Multivalent Charge Carriers. In *Encyclopedia of Electrochemistry: Batteries*; Wiley, 2020; pp 1–36. https://doi.org/10.1002/9783527610426.bard110020.

(7) Guo, D.; Shi, Z.; El-Demellawi, J. K.; Wahyudi, W.; Arsalan, M.; Zhang, H.; Alshareef, H. N. Lithium Metal Batteries for High Temperature Environments. *Adv. Energy Mater.* **2025**, *15*, e02943. https://doi.org/10.1002/aenm.202502943.

(8) Feng, Y.; Zhou, L.; Ma, H.; Wu, Z.; Zhao, Q.; Li, H.; Zhang, K.; Chen, J. Challenges and Advances in Wide-Temperature Rechargeable Lithium Batteries. *Energy Environ. Sci.* **2022**, *15*, 1711–1759. https://doi.org/10.1039/d1ee03292e.

(9) Ponrouch, A.; Bitenc, J.; Dominko, R.; Lindahl, N.; Johansson, P.; Palacin, M. R. Multivalent Rechargeable Batteries. *Energy Storage Mater.* **2019**, *20* (February), 253–262. https://doi.org/10.1016/j.ensm.2019.04.012.

(10) Forero-Saboya, J.; Davoisne, C.; Dedryvère, R.; Yousef, I.; Canepa, P.; Ponrouch, A. Understanding the Nature of the Passivation Layer Enabling Reversible Calcium Plating. *Energy Environ. Sci.* **2020**, *13*, 3423–3431. https://doi.org/10.1039/d0ee02347g.

(11) Ponrouch, A.; Rosa Palacín, M. Post-Li Batteries: Promises and Challenges. *Philosophical Transactions of the Royal Society A: Mathematical, Physical and Engineering Sciences* **2019**, *377* (2152). https://doi.org/10.1098/rsta.2018.0297.

(12) Hou, Z.; Zhou, R.; Yao, Y.; Min, Z.; Lu, Z.; Zhu, Y.; Tarascon, J. M.; Zhang, B. Correlation between Electrolyte Chemistry and Solid Electrolyte Interphase for Reversible Ca Metal Anodes. *Angewandte Chemie International Edition* **2022**, *61*, e202214796. https://doi.org/10.1002/ANIE.202214796.

(13) Timhagen, J.; Thangavel, V.; Forero-Saboya, J.; Weidow, J.; Johansson, P. Successes and Failures Predicting the Solubility of Solid Electrolyte Interphase (SEI) Species.

Electrochim. Acta **2025**, *539*, 147051. https://doi.org/10.1016/j.electacta.2025.147051.

(14) Linden, D.; Reddy, T. B.; Beard, K. W. Electricity, Electrochemistry, and Batteries: Prologue and Exposition. In *Linden's Handbook of Batteries*; McGraw Hill Education: United States of America, 2019; pp 3–21.

(15) Gasteiger, H.; Krischer, K.; Scrosati, B. Electrochemical Cells: Basics. In *Lithium Batteries: Advanced Technologies and Applications*; Scrosati, B., Abraham, K. M., van Schalkwijk, W., Hassoun, J., Eds.; John Wiley & Sons, Inc.: Hoboken, New Jersey, USA, 2013; pp 1–19.

(16) Torres, A.; Casals, J. L.; Arroyo-De Dompablo, M. E. Enlisting Potential Cathode Materials for Rechargeable Ca Batteries. *Chemistry of Materials* **2021**, *33* (7), 2488–2497. https://doi.org/10.1021/acs.chemmater.0c04741.

(17) Li, M.; Lu, J.; Ji, X.; Li, Y.; Shao, Y.; Chen, Z.; Zhong, C.; Amine, K. Design Strategies for Nonaqueous Multivalent-Ion and Monovalent-Ion Battery Anodes. *Nature Reviews Materials*. Nature Research April 1, 2020, pp 276–294. https://doi.org/10.1038/s41578-019-0166-4.

(18) Renais, C.; Villevieille, C.; Peljo, P.; El Bachraoui, F.; Girault, H. Redox Aspects of Lithium-Ion Batteries. Is Graphite an Anode? *EES Batteries* **2026**. https://doi.org/10.1039/d5eb00202h.

(19) Xu, K. Lithium-Metal, Lithium-Ion and Other Batteries. In *Electrolytes, Interfaces and Interphases: Fundamentals and Applications in Batteries*; The Royal Society of Chemistry: Craydon, UK, 2023; pp 292–372.

(20) Li, Y.; Lu, Y.; Adelhelm, P.; Titirici, M. M.; Hu, Y. S. Intercalation Chemistry of Graphite: Alkali Metal Ions and Beyond. *Chemical Society Reviews*. Royal Society of Chemistry September 7, 2019, pp 4655–4687. https://doi.org/10.1039/c9cs00162j.

(21) Gummow, R. J.; Vamvounis, G.; Kannan, M. B.; He, Y. Calcium-Ion Batteries: Current State-of-the-Art and Future Perspectives. *Advanced Materials*. Wiley-VCH Verlag September 26, 2018. https://doi.org/10.1002/adma.201801702.

(22) Deng, X.; Li, L.; Zhang, G.; Zhao, X.; Hao, J.; Han, C.; Li, B. Anode Chemistry in Calcium Ion Batteries: A Review. *Energy Storage Mater.* **2022**. https://doi.org/10.1016/J.ENSM.2022.09.033.

(23) Monti, D.; Ponrouch, A.; Araujo, R. B.; Barde, F.; Johansson, P.; Palacín, M. R. Multivalent Batteries-Prospects for High Energy Density: Ca Batteries. *Front. Chem.* **2019**, *7* (FEB), 1–6. https://doi.org/10.3389/fchem.2019.00079.

(24) Nagy, K. S.; Kazemiabnavi, S.; Thornton, K.; Siegel, D. J. Thermodynamic Overpotentials and Nucleation Rates for Electrodeposition on Metal Anodes. *ACS Appl. Mater. Interfaces* **2019**, *11* (8), 7954–7964. https://doi.org/10.1021/acsami.8b19787.

(25) Xu, K. When Electrolyte Meets Electrodes: Interface. In *Electrolytes, Interfaces and Interphases: Fundamentals and Applications in Batteries*; The Royal Society of Chemistry: Craydon, UK, 2023; pp 131–191.

(26) Wang, D.; Gao, X.; Chen, Y.; Jin, L.; Kuss, C.; Bruce, P. G. Plating and Stripping Calcium in an Organic Electrolyte. *Nat. Mater.* **2018**, *17*, 16–20. https://doi.org/10.1038/NMAT5036.

(27) Li, Y.; Kumar, S.; Yang, G.; Lu, J.; Yao, Y.; Kang, K.; Seh, Z. W. The Contrast between Monovalent and Multivalent Metal Battery Anodes. *Science (1979).* **2025**, *390*, 1–11. https://doi.org/10.1126/science.adl5482.

(28) Xu, K. Linking Ionics With Electrodics. In *Electrolytes, Interfaces and Interphases: Fundamentals and Applications in Batteries*; The Royal Society of Chemistry: Craydon, UK, 2023; pp 192–208.

(29) Pu, S. D.; Gong, C.; Gao, X.; Ning, Z.; Yang, S.; Marie, J. J.; Liu, B.; House, R. A.; Hartley, G. O.; Luo, J.; Bruce, P. G.; Robertson, A. W. Current-Density-Dependent Electroplating in Ca Electrolytes: From Globules to Dendrites. *ACS Energy Lett.* **2020**, *5* (7), 2283–2290. https://doi.org/10.1021/acsenergylett.0c01153.

(30) Forero-Saboya, J. D.; Tchitchekova, D. S.; Johansson, P.; Palacín, M. R.; Ponrouch, A. Interfaces and Interphases in Ca and Mg Batteries. *Adv. Mater. Interfaces* **2022**, *9* (8). https://doi.org/10.1002/ADMI.202101578.

(31) Palacin, M. R.; Johansson, P.; Dominko, R.; Dlugatch, B.; Aurbach, D.; Li, Z.; Fichtner, M.; Lužanin, O.; Bitenc, J.; Wei, Z.; Glaser, C.; Janek, J.; Fernández-Barquín, A.; Mainar, A. R.; Leonet, O.; Urdampilleta, I.; Blázquez, J. A.; Tchitchekova, D. S.; Ponrouch, A.; Canepa, P.; Gautam, G. S.; Casilda, R. S. R. G.; Martinez-Cisneros, C. S.; Ureña Torres, N.; Varez, A.; Sanchez, J.-Y.; Kravchyk, K. V; Kovalenko, M. V; Teck, A. A.; Shiel, H.; Stephens, I. E. L.; Ryan, M. P.; Zemlyanushin, E.; Dsoke, S.; Grieco, R.; Patil, N.; Marcilla, R.; Gao, X.; Carmalt, C. J.; He, G.; Titirici, M.-M. Roadmap on Multivalent Batteries. *Journal of Physics: Energy* **2024**. https://doi.org/10.1088/2515-7655/ad34fc.

(32) Lužanin, O.; Moškon, J.; Pavčnik, T.; Dominko, R.; Bitenc, J. Unveiling True Limits of Electrochemical Performance of Organic Cathodes in Multivalent Batteries through Cyclable Symmetric Cells. *Batter. Supercaps* **2023**, *6*, e202200437. https://doi.org/10.1002/batt.202200437.

(33) Slim, Z.; Cruz-Cardona, C.; Pechberty, C.; Hosaka, T.; Mandić, Z.; Panic, V.; Johansson, P. Solvent-Mediated Electrolyte Design for Calcium Metal Batteries.*ACS Mater. Lett.* **2025**, *7*, 3235–3242. https://doi.org/10.1021/acsmaterialslett.5c00892.

(34) Xu, K. When an Electrode Operates Beyond Electrolyte Stability Limits: Interphase. In *Electrolytes, Interfaces and Interphases: Fundamentals and Applications in Batteries*; The Royal Society of Chemistry: Craydon, UK, 2023; pp 209–222.

(35) Xu, K. Electrolytes and Interphases in Li-Ion Batteries and Beyond. *Chem. Rev.* **2014**, *114* (23), 11503–11618. https://doi.org/10.1021/cr500003w.

(36) Forero-Saboya, Juan. D.; Marchante, E.; Araujo, R. B.; Monti, D.; Johansson, P.; Ponrouch, A. Cation Solvation and Physicochemical Properties of Ca Battery Electrolytes. *Journal of Physical Chemistry C* **2019**, *123*, 29524–29532. https://doi.org/10.1021/acs.jpcc.9b07308.

(37) Hou, S.; Ji, X.; Gaskell, K.; Wang, P.; Wang, L.; Xu, J.; Sun, R.; Borodin, O.; Wang, C. *Solvation Sheath Reorganization Enables Divalent Metal Batteries with Fast Interfacial Charge Transfer Kinetics*; 2021; Vol. 374. https://www.science.org.

(38) Peled, E. The Electrochemical Behavior of Alkali and Alkaline Earth Metals in Nonaqueous Battery Systems-The Solid Electrolyte Interphase Model. *J. Electrochem. Soc.* **1979**, *126* (12), 2047–2051. https://doi.org/https://doi.org/10.1149/1.2128859.

(39) Peljo, P.; Girault, H. H. Electrochemical Potential Window of Battery Electrolytes: The HOMO-LUMO Misconception. *Energy Environ. Sci.* **2018**, *11* (9), 2306–2309. https://doi.org/10.1039/c8ee01286e.
(40) Reiss, H. *The Fermi Level and the Redox Potential*; 1985; Vol. 89. https://pubs.acs.org/sharingguidelines.
(41) Xu, K. Interphases. In *Electrolytes, Interfaces and Interphases: Fundamentals and Applications in Batteries*; The Royal Society of Chemistry: Craydon, UK, 2023; pp 602–713.
(42) Ye, L.; Liao, M.; Zhang, K.; Zheng, M.; Jiang, Y.; Cheng, X.; Wang, C.; Xu, Q.; Tang, C.; Li, P.; Wen, Y.; Xu, Y.; Sun, X.; Chen, P.; Sun, H.; Gao, Y.; Zhang, Y.; Wang, B.; Lu, J.; Zhou, H.; Wang, Y.; Xia, Y.; Xu, X.; Peng, H. A Rechargeable Calcium–Oxygen Battery That Operates at Room Temperature. *Nature* **2024**, *626*, 313–318. https://doi.org/10.1038/s41586-023-06949-x.
(43) Gui, X.; Liu, J.; Zhang, Y.; Li, Y.; Wang, L.; Chong, B.; Kong, X.; Wang, J. A New Interphase Enabled by CaI and Ca(BH4)2 for Reversible Calcium Metal Anodes. *Chemical Communications* **2025**. https://doi.org/10.1039/D5CC03621F.
(44) Liang, J.; Wang, M.; Zhu, S.; Zhu, D.; Wang, R.; Wang, J.; Cui, L.; Huang, M.; Zhang, W.; An, Q.; Zhang, L.; Zhao, K. Corrosion of Calcium Metal in Ca(TFSI)2/DMAc Electrolyte and Its Solution via Alloy Interface and Competitive Solvation. *Angewandte Chemie International Edition* **2025**. https://doi.org/10.1002/anie.202502729.
(45) Xu, K. Ion Solvation. In *Electrolytes, Interfaces and Interphases: Fundamentals and Applications in Batteries*; The Royal Society of Chemistry: Craydon, UK, 2023; pp 400–434.
(46) Chaban, V. Solvation of the Fluorine Containing Anions and Their Lithium Salts in Propylene Carbonate and Dimethoxyethane. *J. Mol. Model.* **2015**, *21* (7). https://doi.org/10.1007/s00894-015-2717-y.
(47) Von Wald Cresce, A.; Gobet, M.; Borodin, O.; Peng, J.; Russell, S. M.; Wikner, E.; Fu, A.; Hu, L.; Lee, H. S.; Zhang, Z.; Yang, X. Q.; Greenbaum, S.; Amine, K.; Xu, K. Anion Solvation in Carbonate-Based Electrolytes. *Journal of Physical Chemistry C* **2015**, *119* (49), 27255–27264. https://doi.org/10.1021/acs.jpcc.5b08895.
(48) Xu, K. Modern Electrolytes. In *Electrolytes, Interfaces and Interphases: Fundamentals and Applications in Batteries*; The Royal Society of Chemistry: Croydon, UK, 2023; pp 6–10.
(49) Yamada, Y.; Yamada, A. Review—Superconcentrated Electrolytes for Lithium Batteries. *J. Electrochem. Soc.* **2015**, *162* (14), A2406–A2423. https://doi.org/10.1149/2.0041514jes.
(50) Xu, K. Ion Transport in Electrolytes. In *Electrolytes, Interfaces and Interphases: Fundamentals and Applications in Batteries*; The Royal Society of Chemistry: Craydon, UK, 2023; pp 65–130.
(51) Xu, K. Quantification of Ion-Ion Interaction: Debye-Hückel Theory. In *Electrolytes, Interfaces and Interphases: Fundamentals and Applications in Batteries*; The Royal Society of Chemistry: Croydon, UK, 2023; pp 29–64.
(52) Gouverneur, M.; Schmidt, F.; Schönhoff, M. Negative Effective Li Transference Numbers in Li Salt/Ionic Liquid Mixtures: Does Li Drift in the “Wrong” Direction?

Physical Chemistry Chemical Physics **2018**, *20* (11), 7470–7478. https://doi.org/10.1039/c7cp08580j.

(53) Walz, M. M.; van der Spoel, D. Microscopic Origins of Conductivity in Molten Salts Unraveled by Computer Simulations. *Commun. Chem.* **2021**, *4*, 1–10. https://doi.org/10.1038/s42004-020-00446-2.

(54) Forero-Saboya, J. D.; Lozinšek, M.; Ponrouch, A. Towards Dry and Contaminant Free Ca(BF4)2-Based Electrolytes for Ca Plating. *Journal of Power Sources Advances* **2020**, *6*, 100032. https://doi.org/10.1016/j.powera.2020.100032.

(55) Li, Z.; Fuhr, O.; Fichtner, M.; Zhao-Karger, Z. Towards Stable and Efficient Electrolytes for Room-Temperature Rechargeable Calcium Batteries. *Energy Environ. Sci* **2019**, *12*, 3496–3501. https://doi.org/10.1039/c9ee01699f.

(56) Shyamsunder, A.; Blanc, L. E.; Assoud, A.; Nazar, L. F. Reversible Calcium Plating and Stripping at Room Temperature Using a Borate Salt. *ACS Energy Lett.* **2019**, *4*, 2271–2276. https://doi.org/10.1021/ACSENERGYLETT.9B01550.

(57) Nielson, K. V.; Luo, J.; Liu, T. L. Optimizing Calcium Electrolytes by Solvent Manipulation for Calcium Batteries. *Batter. Supercaps* **2020**, *3*, 766–772. https://doi.org/10.1002/BATT.202000005.

(58) Yi, Y.; Xing, Y.; Wang, H.; Zeng, Z.; Sun, Z.; Li, R.; Lin, H.; Ma, Y.; Pu, X.; Li, M. M.-J.; Park, K.-Y.; Xu, Z.-L. Deciphering Anion-Modulated Solvation Structure for Calcium Intercalation into Graphite for Ca-Ion Batteries. *Angewandte Chemie International Edition* **2024**, *63*, e202317177. https://doi.org/10.1002/anie.202317177.

(59) Jie, Y.; Tan, Y.; Li, L.; Han, Y.; Xu, S.; Zhao, Z.; Cao, R.; Ren, X.; Huang, F.; Lei, Z.; Tao, G.; Zhang, G.; Jiao, S. Electrolyte Solvation Manipulation Enables Unprecedented Room-Temperature Calcium-Metal Batteries. *Angewandte Chemie - International Edition* **2020**, *59*, 12689–12693. https://doi.org/10.1002/ANIE.202002274.

(60) Kisu, K.; Dorai, A.; Hatakeyama-Sato, K.; Takano, T.; Takagi, S.; Oyaizu, K.; Orimo, S. I. Enhanced Durability of Ca Metal Battery with Dual Salt: Synergistic Effect on Solid Electrolyte Interphase and Solvation Structure for Improved Electrodeposition. *ACS Appl. Mater. Interfaces* **2024**, *17*, 1322–1331. https://doi.org/10.1021/acsami.4c18599.

(61) Song, H.; Li, Y.; Tian, F.; Wang, C. Electrolyte Optimization and Interphase Regulation for Significantly Enhanced Storage Capability in Ca-Metal Batteries. *Adv. Funct. Mater.* **2022**, *32*, 2200004. https://doi.org/10.1002/ADFM.202200004.

(62) Song, H.; Su, J.; Wang, C. Multi-Ions Electrolyte Enabled High Performance Voltage Tailorable Room-Temperature Ca-Metal Batteries. *Adv. Energy Mater.* **2021**, *11*, 2003685. https://doi.org/10.1002/aenm.202003685.

(63) Tchitchekova, D. S.; Monti, D.; Johansson, P.; Bardé, F.; Randon-Vitanova, A.; Palacín, M. R.; Ponrouch, A. On the Reliability of Half-Cell Tests for Monovalent (Li+, Na+) and Divalent (Mg2+, Ca2+) Cation Based Batteries. *J. Electrochem. Soc.* **2017**, *164*, 1384–1392. https://doi.org/10.1149/2.0411707jes.

(64) Okoshi, M.; Yamada, Y.; Komaba, S.; Yamada, A.; Nakai, H. Theoretical Analysis of Interactions between Potassium Ions and Organic Electrolyte Solvents: A Comparison with Lithium, Sodium, and Magnesium Ions. *J. Electrochem. Soc.* **2017**, *164*, A54–A60. https://doi.org/10.1149/2.0211702jes.

(65) Chando, P. A.; Shellhamer, J. M.; Wall, E.; He, W.; Hosein, I. D. Plating and Stripping Calcium Metal in Potassium Hexafluorophosphate Electrolyte toward a Stable Hybrid Solid Electrolyte Interphase. *ACS Appl. Energy Mater.* **2023**, *6*, 3924–3932. https://doi.org/10.1021/acsaem.3c00098.

(66) Song, H.; Su, J.; Wang, C. Hybrid Solid Electrolyte Interphases Enabled Ultralong Life Ca–Metal Batteries Working at Room Temperature. *Advanced Materials* **2020**, No. 33, 2006141. https://doi.org/10.1002/ADMA.202006141.

(67) Welton, T. Ionic Liquids: A Brief History. *Biophys. Rev.* **2018**, *10* (3), 691–706. https://doi.org/10.1007/S12551-018-0419-2/SCHEMES/3.

(68) Wilkes, J. S. A Short History of Ionic Liquids - From Molten Salts to Neoteric Solvents. *Green Chemistry* **2002**, *4* (2), 73–80. https://doi.org/10.1039/b110838g.

(69) Sharma, S.; Ivanov, A. S.; Margulis, C. J. A Brief Guide to the Structure of High-Temperature Molten Salts and Key Aspects Making Them Different from Their Low-Temperature Relatives, the Ionic Liquids. *J. Phys. Chem. B* **2021**, *125*, 43. https://doi.org/10.1021/acs.jpcb.1c01065.

(70) Nohira, T. Novel Electrochemical Reactions in Molten Salts and Ionic Liquids and Their Applications. *Electrochemistry* **2020**, *88* (6), 477–488. https://doi.org/10.5796/ELECTROCHEMISTRY.20-00098.

(71) Giordani, V.; Tozier, D.; Tan, H.; Burke, C. M.; Gallant, B. M.; Uddin, J.; Greer, J. R.; Mccloskey, B. D.; Chase, G. V; Addison, D. A Molten Salt Lithium−Oxygen Battery. *J. Am. Chem. Soc.* **2016**, *138*, 2656–2663. https://doi.org/10.1021/jacs.5b11744.

(72) Zhou, H.; Li, H.; Gong, Q.; Yan, S.; Zhou, X.; Liang, S.; Ding, W.; He, Y.; Jiang, K.; Wang, K. A Sodium Liquid Metal Battery Based on the Multi-Cationic Electrolyte for Grid Energy Storage. *Energy Storage Mater.* **2022**, *50*, 572–579. https://doi.org/10.1016/j.ensm.2022.05.032.

(73) Ding, W.; Gong, Q.; Liang, S.; Hoffmann, R.; Zhou, H.; Li, H.; Wang, K.; Zhang, T.; Weisenburger, A.; Müller, G.; Bonk, A. Multi-Cationic Molten Salt Electrolyte of High-Performance Sodium Liquid Metal Battery for Grid Storage. *J. Power Sources* **2023**, *553*, 232254. https://doi.org/10.1016/J.JPOWSOUR.2022.232254.

(74) Song, Y.; Jiao, S.; Tu, J.; Wang, J.; Liu, Y.; Jiao, H.; Mao, X.; Guo, Z.; Fray, D. J. A Long-Life Rechargeable Al Ion Battery Based on Molten Salts †. **2017**. https://doi.org/10.1039/c6ta09829k.

(75) Pang, Q.; Meng, J.; Gupta, S.; Hong, X.; Yuen Kwok, C.; Zhao, J.; Jin, Y.; Xu, L.; Karahan, O.; Wang, Z.; Toll, S.; Mai, L.; Nazar, L. F.; Balasubramanian, M.; Narayanan, B.; Sadoway, D. R. Fast-Charging Aluminium-Chalcogen Batteries Resistant to Dendritic Shorting. *Nature* **2022**, *608*, 704–711. https://doi.org/10.1038/s41586-022-04983-9.

(76) Hagiwara, R.; Tamaki, K.; Kubota, K.; Goto, T.; Nohira, T. Thermal Properties of Mixed Alkali Bis(Trifluoromethylsulfonyl)Amides. *J. Chem. Eng. Data* **2008**, *53* (2), 355–358. https://doi.org/10.1021/je700368r.

(77) Kubota, K.; Nohira, T.; Goto, T.; Hagiwara, R. Ternary Phase Diagrams of Alkali Bis(Trifluoromethylsulfonyl)Amides. *J. Chem. Eng. Data* **2008**, *53* (9), 2144–2147. https://doi.org/10.1021/je800292f.

(78) Kubota, K.; Tamaki, K.; Nohira, T.; Goto, T.; Hagiwara, R. Electrochemical Properties of Alkali Bis(Trifluoromethylsulfonyl)Amides and Their Eutectic Mixtures. *Electrochim. Acta* **2010**, *55*, 1113–1119. https://doi.org/10.1016/j.electacta.2009.09.024.
(79) Kubota, K.; Nohira, T.; Goto, T.; Hagiwara, R. Novel Inorganic Ionic Liquids Possessing Low Melting Temperatures and Wide Electrochemical Windows: Binary Mixtures of Alkali Bis(Fluorosulfonyl)Amides. *Electrochem. commun.* **2008**, *10* (12), 1886–1888. https://doi.org/10.1016/j.elecom.2008.10.001.
(80) Kubota, K.; Nohira, T.; Takuya, G.; Hagiwara, R. Binary and Ternary Mixtures of MFSA (M = Li, K, Cs) as New Inorganic Ionic Liquids. *ECS Trans.* **2009**, *16* (24), 91–98. https://doi.org/10.1149/1.3109636.
(81) Kubota, K.; Nohira, T.; Hagiwara, R. Thermal Properties of Alkali Bis(Fluorosulfonyl)Amides and Their Binary Mixtures. *J. Chem. Eng. Data* **2010**, *55* (9), 3142–3146. https://doi.org/10.1021/je9010932.
(82) Kubota, K.; Nohira, T.; Hagiwara, R. New Inorganic Ionic Liquids Possessing Low Melting Temperatures and Wide Electrochemical Windows: Ternary Mixtures of Alkali Bis(Fluorosulfonyl)Amides. *Electrochim. Acta* **2012**, *66*, 320–324. https://doi.org/10.1016/j.electacta.2012.01.097.
(83) Yan, S.; Yao, N.; Liu, H.; Zhang, Z.; Lu, Y.; Liu, Z.; Hou, W.; Zhou, P.; Zhou, H.; Chen, X.; Liu, K.; Zhang, Q. Molten Salt Electrolytes with Enhanced Li+-Transport Kinetics for Fast-Cycling of High-Temperature Lithium Metal Batteries. *Energy Environ. Sci.* **2025**, *18*, 1696–1706. https://doi.org/10.1039/d4ee04657a.
(84) Kubota, K.; Nohira, T.; Rika, H.; Hajime, M. Thermal Properties of Alkali (Fluorosulfonyl)(Trifluoromethylsulfonyl)Amides. *Chem. Lett.* **2010**, *39* (12), 1303–1304. https://doi.org/10.1246/cl.2010.1303.
(85) Kubota, K.; Matsumoto, H. Melting and Crystallization Behaviors of Alkali Metal (Fluorosulfonyl) (Trifluoromethylsulfonyl)Amides. *Chem. Lett.* **2011**, *40* (10), 1105–1106. https://doi.org/10.1246/cl.2011.1105.
(86) Kubota, K.; Matsumoto, H. Investigation of an Intermediate Temperature Molten Lithium Salt Based on Fluorosulfonyl(Trifluoromethylsulfonyl)Amide as a Solvent-Free Lithium Battery Electrolyte. *Journal of Physical Chemistry C* **2013**, *117* (37), 18829–18836. https://doi.org/10.1021/jp405068q.
(87) Kubota, K.; Matsumoto, H. Cation Mixtures of Alkali Metal (Fluorosulfonyl)(Trifluoromethylsulfonyl)Amide as Electrolytes for Lithium Secondary Battery. *J. Electrochem. Soc.* **2014**, *161* (6), A902–A907. https://doi.org/10.1149/2.026406jes.
(88) Kubota, K.; Matsumoto, H. Lithium Molten Salt Battery at Near Room Temperature Using Low-Melting Alkali Metal Melts. *ECS Trans.* **2016**, *73* (1), 95–100. https://doi.org/10.1149/07301.0095ecst.
(89) Ouchi, T.; Kim, H.; Spatocco, B. L.; Sadoway, D. R. Calcium-Based Multi-Element Chemistry for Grid-Scale Electrochemical Energy Storage. *Nat. Commun.* **2016**, *7*. https://doi.org/10.1038/ncomms10999.
(90) Dickson, S. A. M.; Gover, R. K. B.; Irvine, J. T. S. Development of the Ca/FeS2Chemistry for Thermal Batteries. *Chemistry of Materials* **2021**, *33* (18), 7367–7378. https://doi.org/10.1021/acs.chemmater.1c01864.

(91) Fernández, A. G.; Ushak, S.; Galleguillos, H.; Pérez, F. J. Development of New Molten Salts with LiNO3 and Ca(NO3)2 for Energy Storage in CSP Plants. *Appl. Energy* **2014**, *119*, 131–140. https://doi.org/10.1016/j.apenergy.2013.12.061.
(92) Cai, Y.; Zhang, H.; Cao, Y.; Wang, Q.; Cao, B.; Zhou, Z.; Lv, F.; Song, W.; Duo, D.; Yu, L. Synthesis, Application and Industrialization of LiFSI: A Review and Perspective. *J. Power Sources* **2022**, *535*, 231481. https://doi.org/10.1016/j.jpowsour.2022.231481.
(93) Yeh, J. W.; Chen, S. K.; Lin, S. J.; Gan, J. Y.; Chin, T. S.; Shun, T. T.; Tsau, C. H.; Chang, S. Y. Nanostructured High-Entropy Alloys with Multiple Principal Elements: Novel Alloy Design Concepts and Outcomes. *Adv. Eng. Mater.* **2004**, *6* (5), 299–303. https://doi.org/10.1002/adem.200300567.
(94) Murty, B. S.; Yeh, J. W.; Ranganathan, S.; Bhattacharjee, P. P. *High-Entropy Alloys*, Second Edition.; Elsevier, 2019.
(95) Oses, C.; Toher, C.; Curtarolo, S. High-Entropy Ceramics. *Nature Reviews Materials*. Nature Research April 1, 2020, pp 295–309. https://doi.org/10.1038/s41578-019-0170-8.
(96) Amiri, A.; Shahbazian-Yassar, R. Recent Progress of High-Entropy Materials for Energy Storage and Conversion. *Journal of Materials Chemistry A*. Royal Society of Chemistry January 14, 2021, pp 782–823. https://doi.org/10.1039/d0ta09578h.
(97) Zhang, W.; Xia, H.; Zhu, Z.; Lv, Z.; Cao, S.; Wei, J.; Luo, Y.; Xiao, Y.; Liu, L.; Chen, X. Decimal Solvent-Based High-Entropy Electrolyte Enabling the Extended Survival Temperature of Lithium-Ion Batteries to −130 °C. *CCS Chemistry* **2021**, *3* (4), 1245–1255. https://doi.org/10.31635/CCSCHEM.020.202000341.
(98) Kim, S. C.; Wang, J.; Xu, R.; Zhang, P.; Chen, Y.; Huang, Z.; Yang, Y.; Yu, Z.; Oyakhire, S. T.; Zhang, W.; Greenburg, L. C.; Kim, M. S.; Boyle, D. T.; Sayavong, P.; Ye, Y.; Qin, J.; Bao, Z.; Cui, Y. High-Entropy Electrolytes for Practical Lithium Metal Batteries. *Nat. Energy* **2023**. https://doi.org/10.1038/s41560-023-01280-1.
(99) Wang, Q.; Zhao, C.; Wang, J.; Yao, Z.; Wang, S.; Kumar, S. G. H.; Ganapathy, S.; Eustace, S.; Bai, X.; Li, B.; Wagemaker, M. High Entropy Liquid Electrolytes for Lithium Batteries. *Nat. Commun.* **2023**, *14* (1). https://doi.org/10.1038/s41467-023-36075-1.
(100) Wang, Q.; Zhao, C.; Yao, Z.; Wang, J.; Wu, F.; Kumar, S. G. H.; Ganapathy, S.; Eustace, S.; Bai, X.; Li, B.; Lu, J.; Wagemaker, M. Entropy-Driven Liquid Electrolytes for Lithium Batteries. *Advanced Materials* **2023**, *35* (17). https://doi.org/10.1002/adma.202210677.
(101) Kim, S. C.; Wang, J.; Xu, R.; Zhang, P.; Chen, Y.; Huang, Z.; Yang, Y.; Yu, Z.; Oyakhire, S. T.; Zhang, W.; Greenburg, L. C.; Kim, M. S.; Boyle, D. T.; Sayavong, P.; Ye, Y.; Qin, J.; Bao, Z.; Cui, Y. Supplementary Information: High-Entropy Electrolytes for Practical Lithium Metal Batteries. *Nat. Energy* **2023**.
(102) Kleppa, O. J. *Thermodynamic Properties of Molten Salt Solutions*; 1977.
(103) Yu, D.; Xue, Z.; Mu, T. Eutectics: Formation, Properties, and Applications. *Chemical Society Reviews*. Royal Society of Chemistry August 7, 2021, pp 8596–8638. https://doi.org/10.1039/d1cs00404b.
(104) Janz, G. J. Physical Properties and Structure of Molten Salts. *J. Chem. Educ.* **1962**, *39* (2), 59–67. https://doi.org/https://doi.org/10.1021/ed039p59.

(105) Heal, G. R. Thermogravimetry and Derivative Thermogravimetry. In *Principles of Thermal Analysis and Calorimetry*; Haines, P. J., Ed.; The Royal Society of Chemistry: Cambridge CB4 0WF, UK, 2002; pp 10–54.
(106) Laye, P. G. Differential Thermal Analysis and Differential Scanning Calorimetry. In *Principles of Thermal Analysis and Calorimetry*; Haines, P. J., Ed.; The Royal Society of Chemistry: Cambridge CB4 0WF, UK, 2002; pp 55–93.
(107) A Guide to On-Line Conductivity Measurement: Theory and Practice Conductivity Guide. Mettler Toledo 2023.
(108) Harris, D. C.; Bertolucci, M. D. *Symmetry and Spectroscopy: An Introduction to Vibrational and Electronic Spectroscopy*; Dover Publication, Inc.: Mineola, NY, Unated Stated of America, 1989.
(109) Dugas, R.; Forero-Saboya, J. D.; Ponrouch, A. Methods and Protocols for Reliable Electrochemical Testing in Post-Li Batteries (Na, K, Mg, and Ca). *Chem.Mater.* **2019**, *31* (21), 8613–8628. https://doi.org/10.1021/acs.chemmater.9b02776.
(110) Bard, A. J.; Faulkner, L. R. *Electrochemical Methods*, Second Edition.; 2001.
(111) Elgrishi, N. N.; Rountree, K. J.; Mccarthy, B. D.; Rountree, E. S.; Eisenhart, T. T.; Dempsey, J. L. A Practical Beginner's Guide to Cyclic Voltammetry. **2017**. https://doi.org/10.1021/acs.jchemed.7b00361.
(112) Cruz, C.; Johansson, P. Local Structure and Dynamics in Solvent-Free Molten Salt Ca2+-Electrolytes. *ChemPhysChem* **2025**, *26*, e202500090. https://doi.org/10.1002/cphc.202500090.
(113) Grondin, J.; Lassègues, J. C.; Cavagnat, D.; Buffeteau, T.; Johansson, P.; Holomb, R. Revisited Vibrational Assignments of Imidazolium-Based Ionic Liquids. *Journal of Raman Spectroscopy* **2011**, *42* (4), 733–743. https://doi.org/10.1002/jrs.2754.
(114) Kimura, K.; Motomatsu, J.; Tominaga, Y. Correlation between Solvation Structure and Ion-Conductive Behavior of Concentrated Poly(Ethylene Carbonate)-Based Electrolytes. *Journal of Physical Chemistry C* **2016**, *120* (23), 12385–12391. https://doi.org/10.1021/acs.jpcc.6b03277.
(115) Wang, J.; Yamada, Y.; Sodeyama, K.; Chiang, C. H.; Tateyama, Y.; Yamada, A. Superconcentrated Electrolytes for a High-Voltage Lithium-Ion Battery. *Nat. Commun.* **2016**, *7*, 12032. https://doi.org/10.1038/ncomms12032.
(116) Matsumoto, K.; Oka, T.; Nohira, T.; Hagiwara, R. Polymorphism of Alkali Bis(Fluorosulfonyl)Amides (M[N(SO2F) 2], M = Na, K, and Cs). *Inorg. Chem.* **2013**, *52*, 568–576. https://doi.org/10.1021/IC3010486/SUPPL_FILE/IC3010486_SI_002.PDF.
(117) Georgopoulos, S. L.; Edwards, H. G. M.; De Oliveira, L. F. C. Raman Spectroscopic Analysis of the Interaction between Squaric Acid and Dimethylsulfoxide. *Spectrochim. Acta A Mol. Biomol. Spectrosc.* **2013**, *111*, 54–61. https://doi.org/10.1016/j.saa.2013.03.052.
(118) Miles, M. G.; Doyle, G.; Cooney, R. P.; Tobias, R. S. Raman and Infrared Spectra and Normal coordinates of the Trifiuoromethanesulfonate and trichloromethanesulfonate Anions*. *Spectrochemica Acta* **1969**, *25*, 1515–1526. https://doi.org/https://doi.org/10.1016/0584-8539(69)80135-2.
(119) Sankarasubramanian, S.; Ramani, V. Dimethyl Sulfoxide-Based Electrolytes for High-Current Potassium-Oxygen Batteries. *Journal of Physical Chemistry C* **2018**, *122* (34), 19319–19327. https://doi.org/10.1021/acs.jpcc.8b03755.

(120) Janz, G. J.; James, D. W. Raman Spectra and Ionic Interactions in Molten Nitrates. *J. Chem. Phys.* **1961**, *35* (2), 739–744. https://doi.org/10.1063/1.1731994.